The Effect of Hydrogen on Zirconium Alloy Properties

Volume I

Authors

Alfred Strasser
Aquarius Services, Sleepy Hollow, NY, USA

Ron Adamson
Zircology Plus, Fremont, CA, USA

Friedrich Garzarolli
Fürth, Germany

A.N.T. INTERNATIONAL®

Advanced Nuclear Technology International
Krongjutarvägen 2C, SE-730 50 Skultuna
Sweden

info@antinternational.com
www.antinternational.com

Disclaimer

The information presented in this report has been compiled and analysed by Advanced Nuclear Technology International Europe AB (ANT International®) and its subcontractors. ANT International has exercised due diligence in this work, but does not warrant the accuracy or completeness of the information. ANT International does not assume any responsibility for any consequences as a result of the use of the information for any party, except a warranty for reasonable technical skill, which is limited to the amount paid for this assignment by each *ZIRAT/IZNA* programme member.

Acronyms and expressions

AECL	Atomic Energy of Canada Limited
ANF	Advanced Nuclar Fuel
ANL	Argonne National Laboratory
ASTM	American Society for Testing and Materials
BWR	Boiling Water Reactor
CALPHAD	Calculation of Phase Diagrams
CANDU	Canadian Deuterium Uranium
CEZUS	Companie Europen Ziconium Ugine Sandvik
CT	Compact Tension (specimen for stress corrosion crack propagation tests)
CW	Cold Worked
CWSR	Cold Work and Stress Relieved
DHC	Delayed Hydride Cracking
DSC	Differential Scanning Calorimetry
DX	Duplex
EB	Electron Beam
EC	Edddy Current
ECBE	Effective Control Blade Exposure
EFPD	Effective Full Power Days
ELS	Extra-Low Sn
FA	Fuel Assembly
FC	Fuel Clad Fuel
GE	General Electric
GNF	Global Nuclear Fuel
GTN	Gurson-Tvergaard-Needleman
HCC	Hydride Continuity Coefficient
HPA	High Performance Alloy
HPU	Hydrogen PickUp
HPUF	Hydrogen PickUp Fraction
HPUF	Hydrogen PickUp Factor
HRT	Hydride Reorientation Treatment
HWC	Hydrogen Water Chemistry
ICM	Internal Conical Mandrel
IP	In-Phase
IZNA	Information on Zirconium Alloys
J-R	J-Resistance
KK	KernKraftwerk
KWU	KraftWerkUnion
LHGR	Linear Heat Generation Rate
LK	Låg corrosion (Low Corrosion in Swedish)
LOCA	Loss of Coolant Accident
LTA	Lead Test Assemblies
LTP	Low Temperature Process
LWR	Light Water Reactor
MDA	Mitsubishi Developed Alloy
MHI	Mitsubishi Heavy Industries
NDA	New Developed Alloy
NFIR	Nuclear Fuel Industry Research
NMCA	Noble Metal Chemical Addition
NRC	Nuclear Regulatory Commission
NSRR	Nuclear Safety Research Reactor
NUPEC	NUclear Power Engineering Corporation
NWC	Normal Water Chemistry

OD	Outer Diameter
OIC	Outside-In-Cracking
OP	Of-Phase
PCI	Pellet Cladding Interaction
PCMI	Pellet Cladding Mechanical Interaction
PIE	Post-Irradiation Examinations
PLT	Pin Loaded Tensile
PSI	Paul Schrerrer Institute
PT	Pressure Tube
PWR	Pressurised Water Reactor
RCT	Ring Compression Rest
RHT	Radial Hydride Treatment
RIA	Reactivity Initiated Accident
RX	Recrystallised
RXA	Recrystallised Annealed
SAT	Slotted Arc Test
SEM	Scanning Electron Microscopy
SPP	Second Phase Particle
SRA	Stress Relieved Annealed
TCE	Total Circumferential Elongation
TEM	Transmission Electron Microscopy
TSS	Terminal Solid Solubility
TT	Tensile Test
UTS	Ultimate Tensile Strength
UTT	Uniaxial Tensile Test
VEC	Vallecitos Embedded Charpy
VVER	Voda Voda Energo Reactor (Russian type PWR)
YS	Yield Strength
ZIRAT	ZIRconium Alloy Technology
ZIRLO	ZIRconium Low Oxidation

Unit conversion

TEMPERATURE		
°C + 273.15 = K		°C*1.8 +32 = °F
T(K)	T(°C)	T(°F)
273	**0**	32
289	16	61
298	25	77
373	**100**	212
473	**200**	392
573	**300**	572
633	360	680
673	**400**	752
773	**500**	932
783	510	950
793	520	968
823	550	1022
833	560	1040
873	**600**	1112
878	605	1121
893	620	1148
923	650	1202
973	**700**	1292
1023	750	1382
1053	780	1436
1073	**800**	1472
1136	863	1585
1143	870	1598
1173	**900**	1652
1273	**1000**	1832
1343	1070	1958
1478	1204	**2200**

Radioactivity	
1 Sv	= 100 Rem
1 Ci	= 3.7 x 10^{10} Bq = 37 GBq
1 Bq	= 1 s^{-1}

MASS	
kg	lbs
0.454	**1**
1	2.20

DISTANCE	
x (µm)	x (mils)
0.6	0.02
1	0.04
5	0.20
10	0.39
20	0.79
25	0.98
25.4	**1.00**
100	3.94

PRESSURE		
bar	MPa	psi
1	0.1	14
10	**1**	142
70	7	995
70.4	7.04	**1000**
100	10	1421
130	13	1847
155	15.5	2203
704	70.4	**10000**
1000	100	14211

STRESS INTENSITY FACTOR	
MPa√m	ksi√inch
0.91	**1**
1	1.10

Contents

1 Introduction

The effect of hydrogen on the properties of zirconium alloys applied to nuclear fuel elements is one of the most significant factors that influence the performance of the alloys at extended burnups. A comprehensive summary and evaluation of the topic is presented in this report.

Volume 1 of the report describes the zirconium-hydrogen system, the characteristics of the hydrides, the pick-up of hydrogen by the alloys during the water corrosion process, the accommodation and distribution of hydrogen in the zirconium alloys, the effect of the hydrogen on the mechanical and physical properties of the alloys and the effect of hydrogen on dimensional stability and corrosion resistance.

Volume 2 of the report describes the effect of hydrogen on the normal and hypothetical accident performance of the zirconium alloy components during reactor operations. The accidents considered include the Loss of Coolant Accident (*LOCA*), the Reactivity Insertion Accident (*RIA*) and those that might occur during dry storage and transportation of spent fuel.

The limited solubility of hydrogen in zirconium is exceeded within the lifetime of the zirconium alloy components and, as a result, zirconium hydrides of various compositions, quantities, distributions and orientations are formed that have a variety of effects on the alloy properties. The primary effect of the hydrides is the decrease of the alloys' ductility concurrent with an increase in its mechanical strength. The hydrides also contribute to dimensional changes of the alloy components and hydride layers on the surface of components may accelerate the corrosion rates.

These properties are affected during their service life by other factors as well, such as temperature, stress, irradiation and features of the alloy microstructure. Since these factors are interactive with those due to hydrogen, it is often difficult to separate and quantify the effects of hydrogen alone and these cases are discussed wherever applicable.

The review includes summaries of some of the most pertinent recent and older data published, but is not meant to be a complete catalogue of the published data. Emphasis is on the results obtained by the various investigators and the variables that affect the resulting data. Editorial comments by the authors are included where they seem warranted.

2 The zirconium-hydrogen system

2.1 Phase diagram and microstructures

The zirconium (Zr) – hydrogen (H) binary equilibrium phase diagram is basic to understanding the relationship between these two elements, Figure 2-1. The solubility of H in Zr at room temperature is essentially zero (< 1 ppm) and increases to only about 200 ppm at operating temperatures (400°C) and as a result a series of hydrides forms at hydrogen levels above the solubility limits. As-fabricated components will all contain some hydrides since their H contents vary in the range of 5-10 ppm.

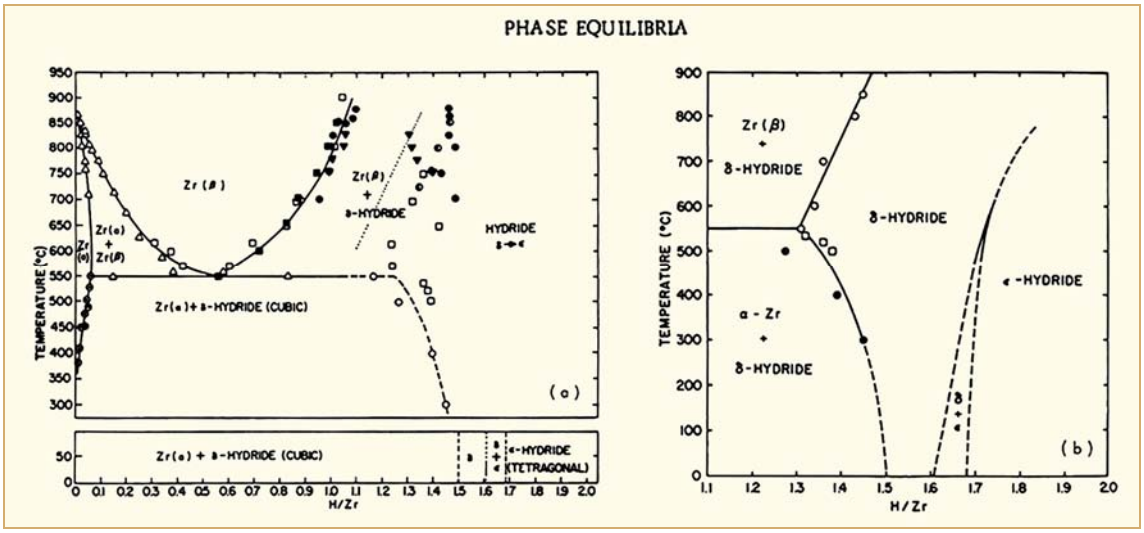

Figure 2-1: (a) Zirconium-hydrogen phase diagram, (b) High hydrogen content portion of the Zr-H phase diagram, Libowitz, 1962.

The three hydrides that have been identified are:

- δ, a face centered cubic crystal structure, and a $ZrH_{1.5}$ to $ZrH_{1.7}$ composition range.
- ε, a body centered tetragonal crystal structure and a wide composition range of $ZrH_{1.7}$ to ZrH_2.
- γ, a body centered tetragonal crystal structure, and the lowest composition range of $ZrH_{1.1}$ to $ZrH_{1.5}$.

The most common hydride observed in irradiated Zr alloy components is δ $ZrH_{1.66}$. The γ phase is believed to be metastable at operating conditions and forms from the δ phase at temperatures below 180°C, Small et al., 1998. As in Figure 2-1, it is often omitted from the phase diagram. However, it has been observed co-existing with δ $ZrH_{1.66}$ and present after heating above and cooling below the terminal solubility limits. The higher oxygen levels in commercial alloys appear to favour the δ over the γ hydride, Cann et al., 1984. The formation and stability of γ hydride has been debated and a good review of this is given by Lanzani & Tuch, 2004.

Recently a new hydride phase has been reported, Zhao et al., 2007. Transmission Electron Microscopy (*TEM*) of Zircaloy-4 containing hydrides formed by either cathodic charging or 360° water corrosion revealed sub-micron size $ZrH_{0.5}$ (or Zr_2H) hydrides, called ζ-hydride, (zeta hydride, see Section 5 for more details). These hydrides are coherent with the matrix and are proposed to be a precursor of the more common gamma or delta hydrides.

Hydrogen is a β stabilizer in Zr (Figure 2-1) and the hydride phases are based on the face centered cubic (fcc) Zr lattice. The γ and ε structures are both distortions of this fcc lattice and their c/a ratios approach 1.0 with temperature; at about >600°C there is only one hydride phase which is cubic and it is an expansion of the theoretical fcc lattice by insertion of H atoms in the tetrahedral interstices - the same structure as δ hydride at room temperature.

The various hydrides and their stoichiometry are identified in samples by x-ray diffraction of their lattice parameters. The δ phase lattice parameter does not change with composition, but the a_o and c_o of the ε phase are strongly influenced and the c/a ratio decreases with increasing H content. The data for the ε phase are shown on Figure 2-2 and the comparison of the two phases on Figure 2-3.

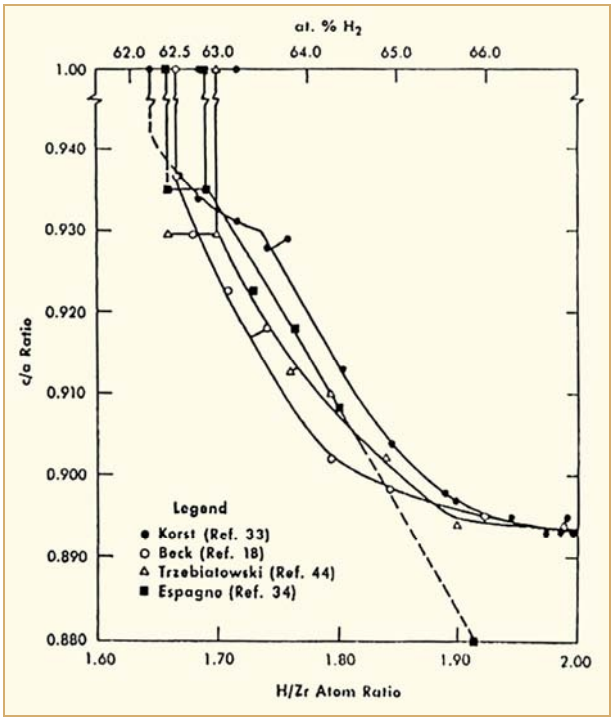

Figure 2-2: Variation in c/a ratio of the epsilon phase with hydrogen content, Mueller et al., 1968.

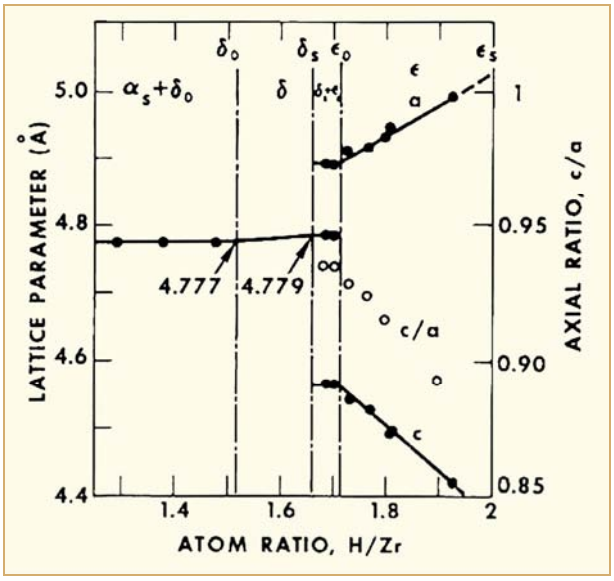

Figure 2-3: Effect of composition on the lattice constants of zirconium hydrides, Espagno et al., 1962.

Careful metallographic examinations show hydrides to be short, thin platelets that have precipitated along a variety of crystallographic planes, on grain boundaries (very common) or intragranularly. For pure zirconium the most common habit plane is near $[10\bar{1}0]$ and for Zircaloy or other alloys it is $[10\bar{1}7]$, which is ~15° from the basal plane. Intragranular precipitation is less common and is more likely to occur in materials with large grain size, at intermetallic particles, at dislocations or as a result of very rapid cooling rates. Factors that determine the orientation of the precipitating hydrides in addition to grain size include stress, texture, and cold work. As a result, the fabrication process will have a strong effect on the hydride orientation as discussed in Section 5. Good reviews of the various hydride precipitates are given by Ells, 1968, Cox & Rudling, 2000 and Coleman, 2003.

As revealed by *TEM*, in annealed material dislocations are often observed around hydrides. Carpenter et al., 1973 has calculated the strains, which occur around hydrides in the zirconium matrix due to the relatively larger volume of the hydride. For δ hydrides the dilatational strains are 7.2%, 4.58% and 4.58% in $[0001]$, $[11\bar{2}0]$ and $[1\bar{1}00]$ directions, thus explaining tendency of a hydride platelet to lie closely to a basal habit plane. The total misfit strain is 16.4%. Note that the partial molar volumes of hydrogen in solution and hydrogen in δ-$ZrH_{1.66}$ are closely the same (Coleman & Ambler, 1983) so there is no net volume charge on precipitation, the lattice dilatational strains due to interstitial hydrogen must be accommodated into the volume converted to hydride, while the zirconium lattice relaxes. This results in the generation of dislocation loops around the hydride platelet, shown in Figure 2-4(a). As described by Coleman, 2003 hydrides are often precipitated close to one another to produce stacks of hydrides that could appear as a long stringer when observed by light microscopy. The elastic strain associated with the precipitation helps nucleate successive precipitates in an autocatalytic process. The dislocation loops and tangles remain when the hydrides are dissolved by heating, and these dislocations may act as nucleation sites for re-precipitation of hydrides on cooling and may affect the apparent precipitation solvus on cooling.

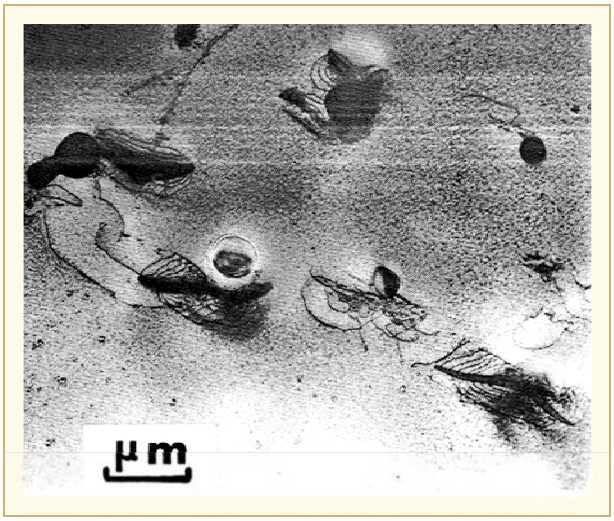

Figure 2-4(a): Dislocation tangles around hydrides, shown in *TEM*, Carpenter et al., 1973.

One should remember that the structures observed at room temperature, during metallographic or other types of structural examinations, are those formed during cool-down from a higher operating or test temperature and may not be completely representative of the structure at the temperature of interest. In fact, the effects of some examination methods have a potential for changing the true representation of the hydrides. A prime example is the etching process of metallographic samples that is likely to produce etch-pits around and between the tips of hydride platelets giving the appearance of a single long platelet. *TEM* has shown that these long stringers are actually a succession of short platelets, Carpenter et al., 1973. Another example is that by reheating samples during the mounting process for metallography, one can nucleate and precipitate hydrides that were not there before, Roy, 1965.

Oxygen, considered both as an impurity and alloying element, has a significant influence on the phase relationships between Zr and H. The majority of the data on the Zr-O-H ternary system were established in the early days of the industry. Knowledge of the system is important because it determines the terminal solubility of H in Zr alloys with their ever present O content in the 1000-1500 ppm range. An early phase diagram shows the 750°C section of the Zr-ZrH_2-ZrO_2 ternary (Figure 2-4(b)), Ells & McQuillan, 1956. According to their work 2 a/o O (3600 ppm) will stabilize the α phase up to 750°C at hydrogen levels up to 50%. At higher H contents more O appears to be required. The data are not without their controversial aspects and a good review and discussion are given by Mueller et al., 1968.

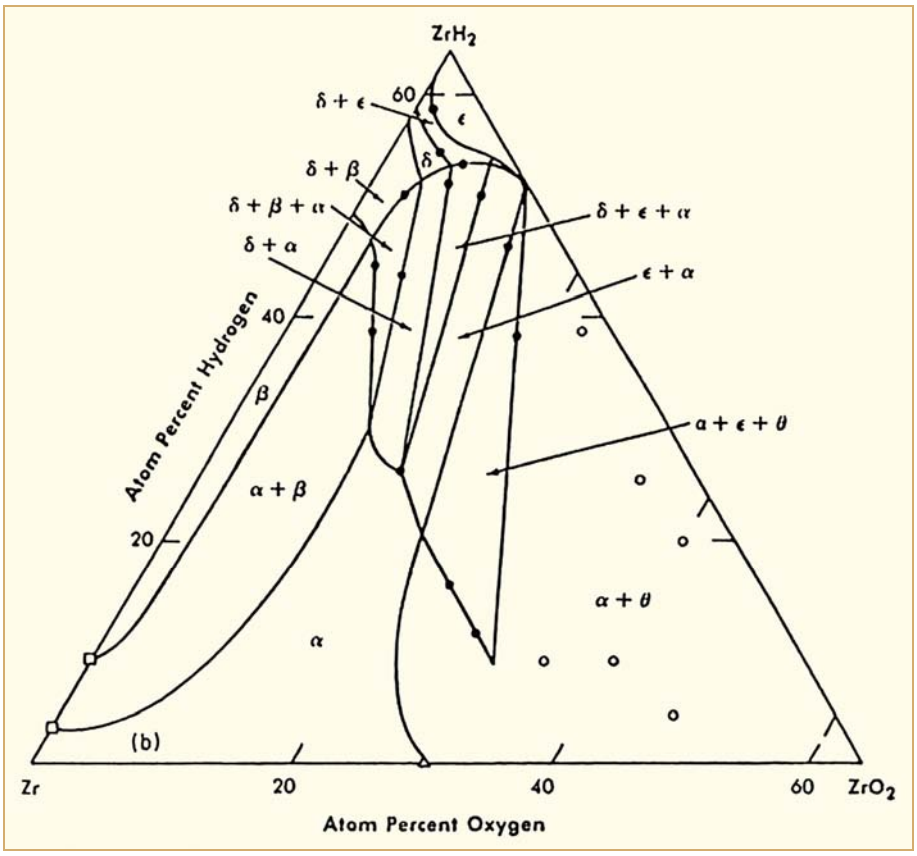

Figure 2-4(b): The Zr-H-O system at 750ºC, Ells & McQuillan, 1956.

A recent Japanese study of the Zr-O-H system consisted of experimental work to determine the 700°C isotherm (Yamanaka et al., 1999(a)) followed by construction of a phase diagram based on calculations using thermodynamic properties with the Calculation of Phase Diagrams (*CALPHAD*) code, Setoyama et al., 2005. The calculations used available property data for the various Zr compounds and the data from the previous experimental work. A comparison of the experimental and calculated isotherms at 700°C is shown Figure 2-5(a) and shows reasonable agreement after some adjustments of the calculated version.

Subsequent calculations show the effect of temperature, H and O content on the α/α+β boundary. Increasing the O content shifts the boundary to the right, stabilizing the α phase and increasing the H solubility, Figure 2-5(b). One should note, however, that this diagram has no experimental foundation below 700°C and this conclusion may be questionable.

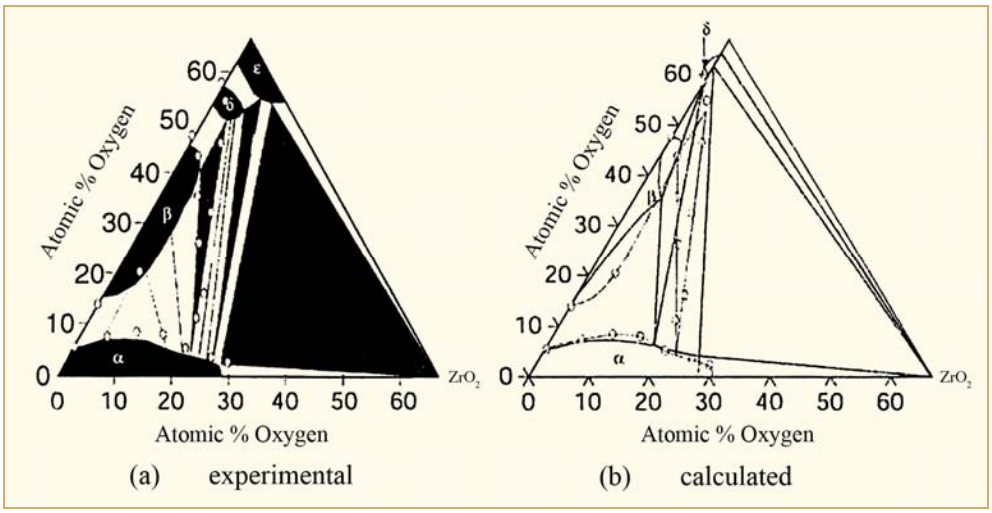

Figure 2-5(a): Isothermal sections of Zr-O-H ternary phase diagram at 700°C. (a) Experimental (b) Setoyama et al., 2005.

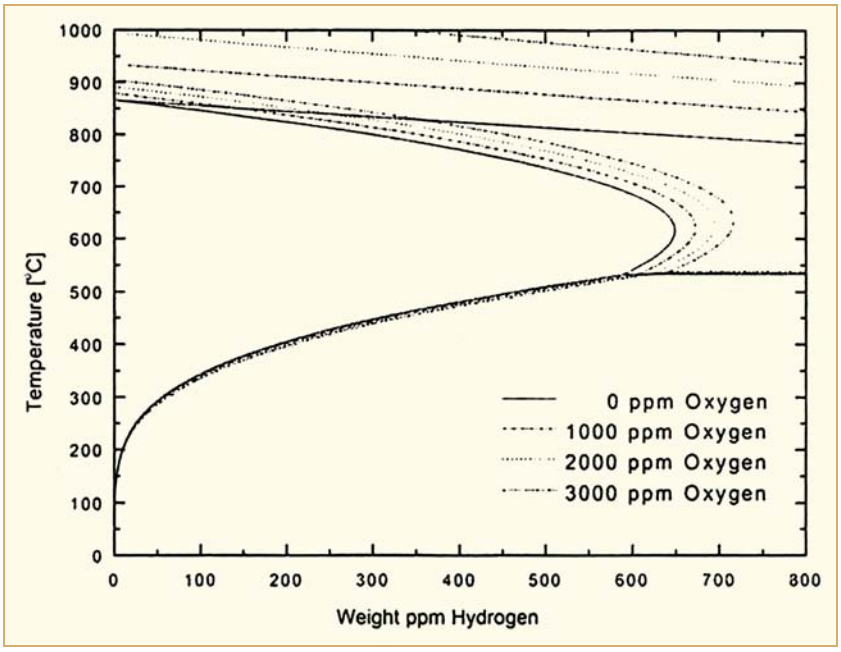

Figure 2-5(b): Calculated pseudo Zr-H(O) phase diagram, Setoyama et al., 2005.

The limitation of the phase diagram work to date is that it does not cover the Zr alloy in-reactor operating temperatures and oxygen contents that adequately apply to fuel assemblies. The significant aspect of this work is that the effect of oxygen level in alloys should be considered when evaluating the solubility and the precipitation of hydrides and perhaps their re-distribution and re-orientation as well. Additional discussion of this topic is in Section 2.2.1, Solubility.

Alloys of practical interest will of course have somewhat different relationships with H than shown by the binary phase diagram; however, the hydrides identified above are applicable to alloys currently in use.

The effects of the alloying elements in the Zircaloys and the Zr-1%Nb alloys on the α→α+β transformation are shown on Figure 2-6 compared to pure Zr. The effect of H content on the transformations between α, α+β and β for the M5 alloy (Zr-1%Nb) is shown on Figure 2-7. Since the end of life H content of M5 is predicted to be well below 300 ppm, the effect of H on the transformation temperatures is expected to be small. It should be noted that the temperatures in these experiments correspond to only a few percent of transformed phase and should not be considered as strictly representative of true equilibrium transus ones (which are considerably lower).

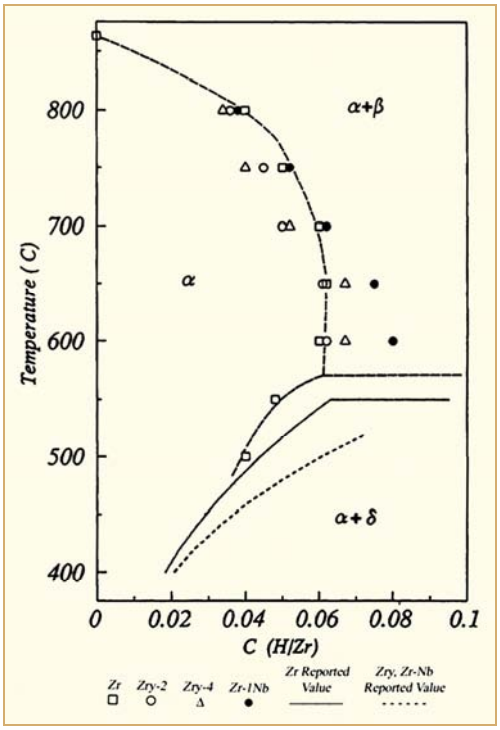

Figure 2-6: Phase boundaries between α and α + β for pure Zr and Zr alloys, Yamanaka et al., 1997.

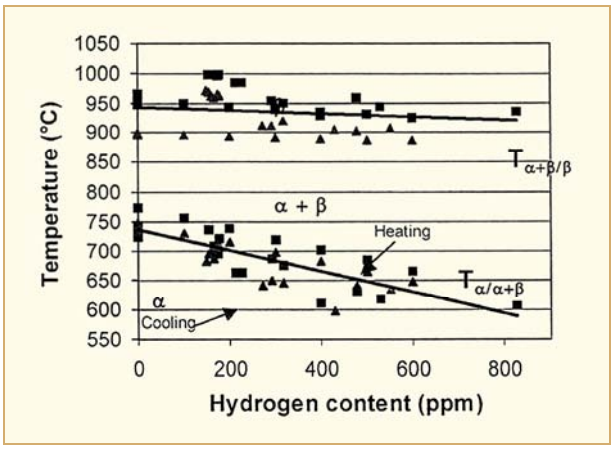

Figure 2-7: Phase transformation temperature of M5 vs. hydrogen content, Mardon et al., 2004.

The effect of alloying elements on H solubility in Zr is discussed in Section 2.2.1.

2.2 Solubility and diffusion of hydrogen

2.2.1 Solubility

Basics

Knowledge of the solubility of H as a function of temperature, time and material characteristics is of great significance to its effect on properties and performance of the Zr alloys. As long as the H levels are within the solubility range, as they may well be at the components' operating temperatures, the H levels will have relatively little effect on properties. Above the solubility range at operating temperatures and during the cool-down to lower temperatures where the solubility drops to essentially zero, the solubility data can have an important influence on properties and performance. Degradation of the material mechanical properties only starts when the hydrides precipitate out of solution.

The solution and the precipitation of the hydrides do not occur at the same temperature as one might expect from the equilibrium phase diagram. The precipitation temperature on cooling is lower than the dissolution temperature on heating because of the supersaturation that occurs during the cooling process. The dissolution temperature is termed the Terminal Solid Solubility temperature (*TSS* or TSS_S or TSS_D), and represents the maximum amount of H that can dissolve without any hydride precipitation. The precipitation temperature is generally identified as TSS_P. The difference between the dissolution and precipitation temperatures is believed to be due to differences in accommodation of the volumetric misfit between the Zr matrix and the less dense hydrides as described in Section 2.1. Plastic accommodation may dominate on heat-up for TSS_D and hydride nucleation with elastic accommodation energy from the hydride misfit might govern TSS_P. Theories based on the heats of solution have also been advanced.

While hydrides dissolve essentially instantaneously, they only precipitate with sufficient supersaturation and this does not occur instantaneously, Kammenzind et al., 1996. The precipitation rate is proportional to the supersaturation: $R_P = \sigma^2(C\text{-}C_{PT})$

where R_P = precipitation rate
σ = fitted parameter
C_{PT} = concentration at which precipitation occurs.

An interesting observation was made some time ago and apparently not corroborated, that thermal cycling increases the solubility of H, Westerman, 1966. The example given was that 30 cycles between 50° and 400°C increased the H solubility in Zircaloy-2. Slow cycling resulted in more supercharging than fast cycling.

Effect of oxygen

The H atoms in solution occupy the tetrahedral sites in the Zr hexagonal close packed crystal structure, indicated as (C) on Figure 2-8(a). Oxygen (O), always present in Zr alloys, occupies the octahedral sites (B), and the interaction between the O and H interstitials affects the H solubility as a function of O content. Increasing occupation of the sites by O decreases the ability to retain H in solid solution. The effect of O on solubility is potentially important, unfortunately available data are conflicting and most relate to higher O contents and temperatures than of interest to fuel element performance. The conclusions of various investigators are summarized next.

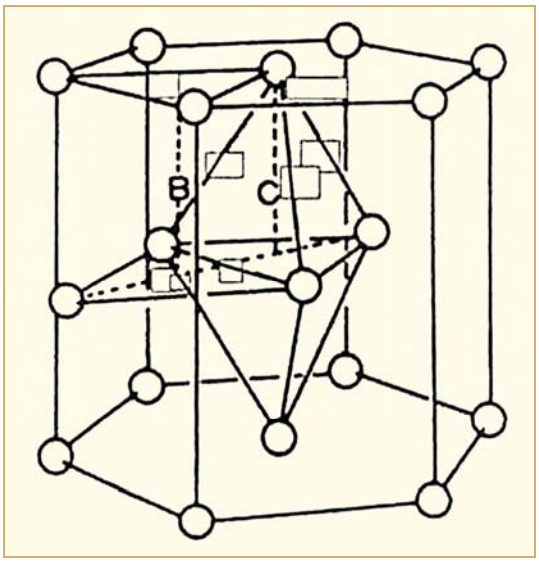

Figure 2-8(a): Zr crystal structure with hydrogen (c) and oxygen (b) in interstial solid solution, Yamanaka et al., 1999(a).

The earliest and some of the best data evaluated the general topic of H solubility in Zr metal and specifically the H solubility in Zr+O solid solutions, Martin & Rees, 1954. Their data show a *decrease in H solubility with increasing O contents up to O/Zr of 1.0 and with increasing temperatures to 820°C, Figure 2-8(b). There is relatively little change in solubility, a slight decrease if any, in the α phase at <1000 ppm O and at 375°C.*

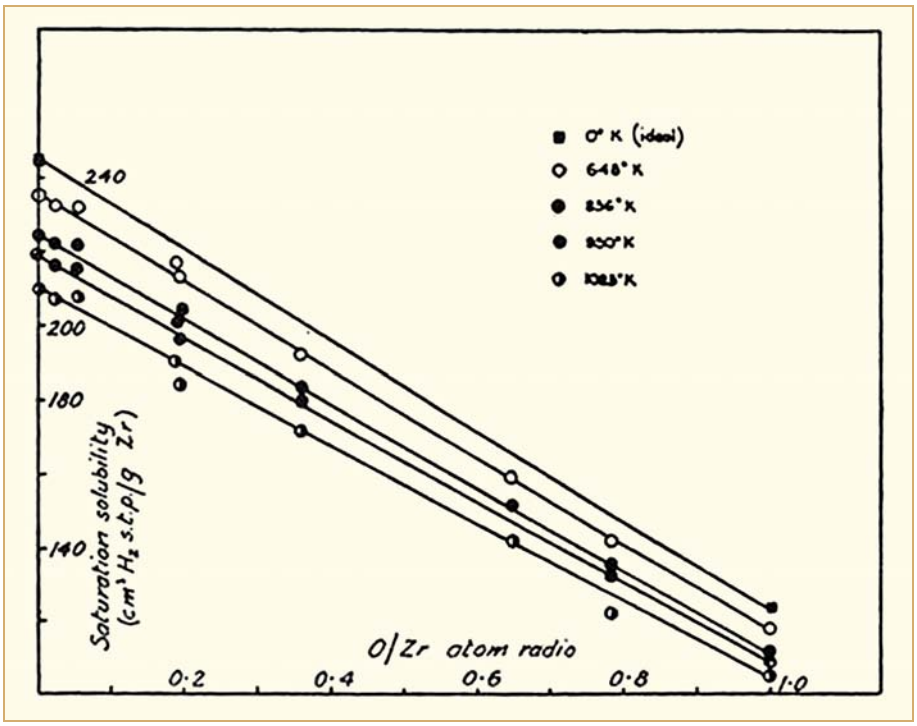

Figure 2-8(b): Experimental points for the saturation solubility as a function of O/Zr atom ratio compared with calculated lines, Martin & Rees, 1954.

Subsequent work measured H solubility in Zr metal with 1200 ppm, 4200 ppm, and 5600 ppm O (and 1.9% Hf!) at 530°-790°C by H pressure measurements and dilatometry, Brown & Hardie, 1961. They *agreed that the H solubility decreased with increasing O content in the β phase, but found that the solubility increased in the α phase.*

A review of the prior data was followed by experiments that oxidized tritium (H^3) containing crystal bar Zr specimens to test whether the O in the octahedral sites blocked H from the neighbouring tetrahedral sites. Samples were oxidized at 500°C and H^3 inserted by re-heating to 800°C, then water quenching or slow cooling. The authors concluded that (1) at the 500°C oxidation the solution of considerable O displaced previously present H, (2) at 800°C H migrated out of the zone enriched even to a small extent by O, (3) at some temperature between 500° and 800°C the H solubility may increase by slight enrichment of the Zr by O. *The experiments confirmed that O does block H from adjacent sites.*

The effect of O as well as alloying elements on the H solubility was studied by pressure measurements and dilatometry, Erickson & Hardie, 1964. The measurements were made with Zr metal containing, 2400 ppm, 3700 ppm 7700 ppm, 9500 ppm (5a/o) and 18500 ppm (9.7a/o%) O alloys in the range of 650° – 800°C. The authors concluded that *the presence of O in solution tends to increase H solubility, but that at low O contents the effect is small.*

A more recent study compared the H solubility and enthalpy of solutions of H in the Zr-O solid solutions Yamanaka et al., 1999(a). The range of compositions examined was from pure Zr to an O/Zr of 0.38 in a temperature range of 400° – 900°C; however, their experiments were very limited at O contents and temperatures of interest. Their conclusions were that *the H solubility in Zr first increased then decreased at the higher O contents.*

The effect of O on *TSS* in Zircaloy-4 was measured by comparing standard TIG welded material containing 1000 to 1200 ppm O with material TIG welded with 0.75% oxygen cover gas that produced material with 2540 to 2860 ppm O, McMinn et al., 2000. The *high O material had a higher solubility for H as shown on the TSS curves on Figure 2-9(a) and this depresses the dissolution and precipitation temperatures.*

These authors conclude that there is general agreement that H solubility decreases with increasing O content in the β phase. The effect of O on the H solubility in the α phase is uncertain at O levels of practical interest and could either increase or decrease. In either case the effect is expected to be small.

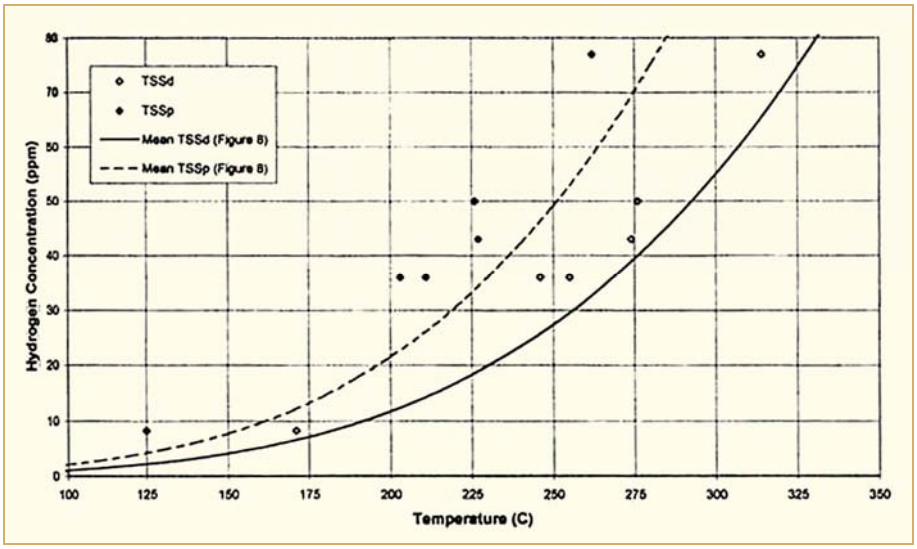

Figure 2-9(a): *TSS* data points for Zircaloy with 2540 to 2860 ppm O compared to Zircaloy with 1000 to 1200 ppm O (solid and dashed curves), McMinn et al., 2000.

Effect of alloying elements

The *solubility of H in pure Zr and in the Zircaloys* was measured in the beginning of the industry's days and these early measurements on unirradiated materials have been validated by more recent data, Kammenzind et al., 1996. The comparison of results by Kammenzind's results are compared to the earlier data on Figure 2-9(b) for TSS_D and Figure 2-10 for TSS_P. A summary of the data that compare the H solubility in various alloys is shown on Figure 2-11.

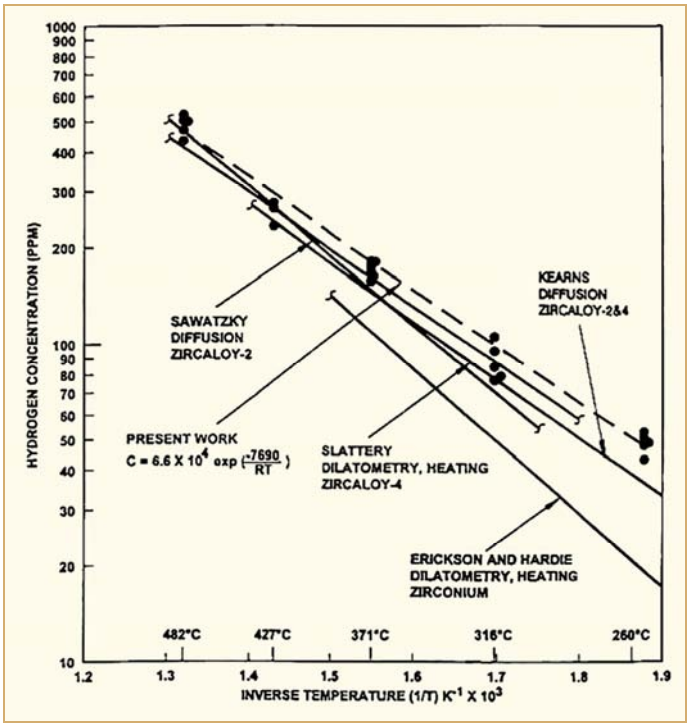

Figure 2-9(b): TSS_D of zirconium and Zircaloys, Kammenzind et al., 1996.

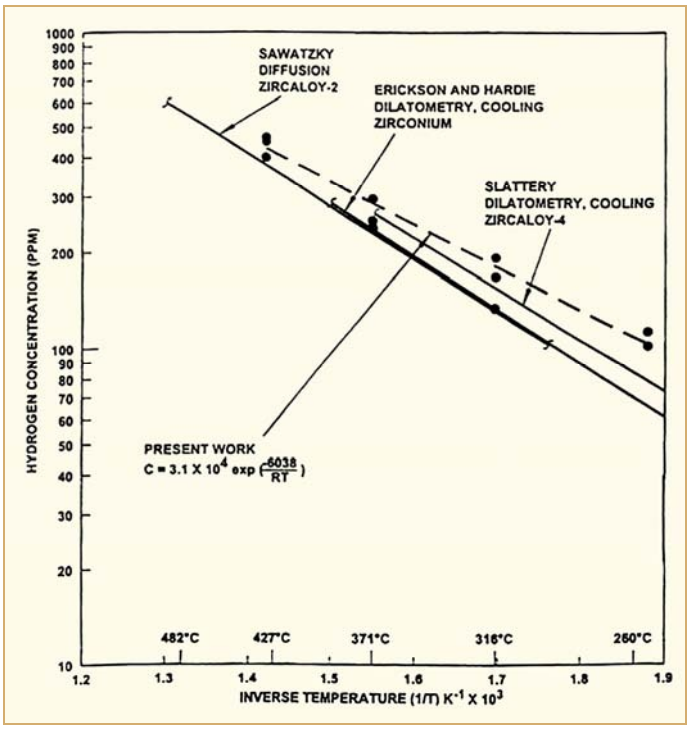

Figure 2-10: *TSS*P of zirconium and Zircaloys, Kammenzind et al., 1996.

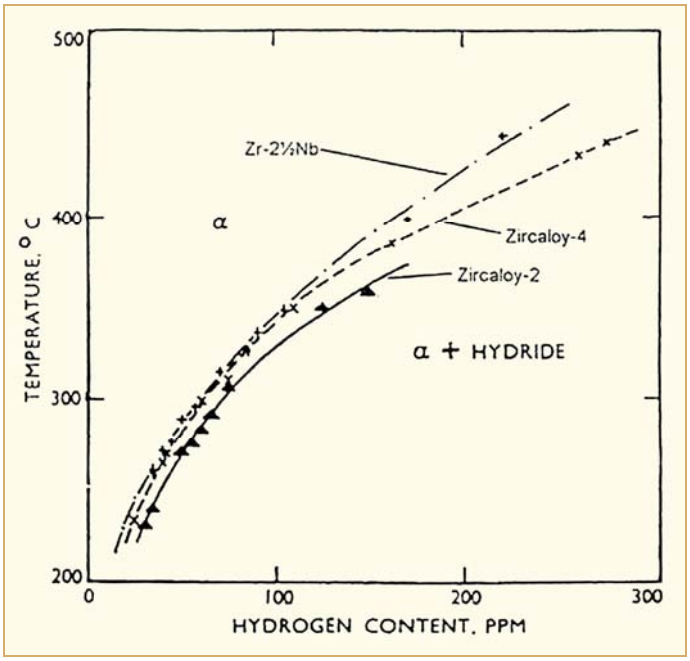

Figure 2-11: Solubility of hydrogen in Zr alloys, Kearns, 1967.

The TSS_D and TSS_P were determined for unirradiated standard and high Fe Zircaloy-2 charged with H in the range of 40-542 ppm by Differential Scanning Calorimetry (*DSC*), Une & Ishimoto, 2003. The comparison of standard, 0.17% Fe, vs. the high, 0.26% Fe alloy was of interest since the high Fe alloy is proposed to have improved corrosion resistance in a Boiling Water Reactor (*BWR*). The results indicate the differential between the dissolution TSS_D and the lower temperature precipitation TSS_P, Figure 2-12. This thermal "hysteresis" is compared to earlier data by other investigators and Zircaloy-4 on Figure 2-13. The TSS_G curve in Figure 2-12 is the growth solvus of hydrides, representing the solubility boundary in the presence of precipitated hydrides that have reached this state as a result of a growth process. This would occur after nucleation has taken place and the temperature approached from above.

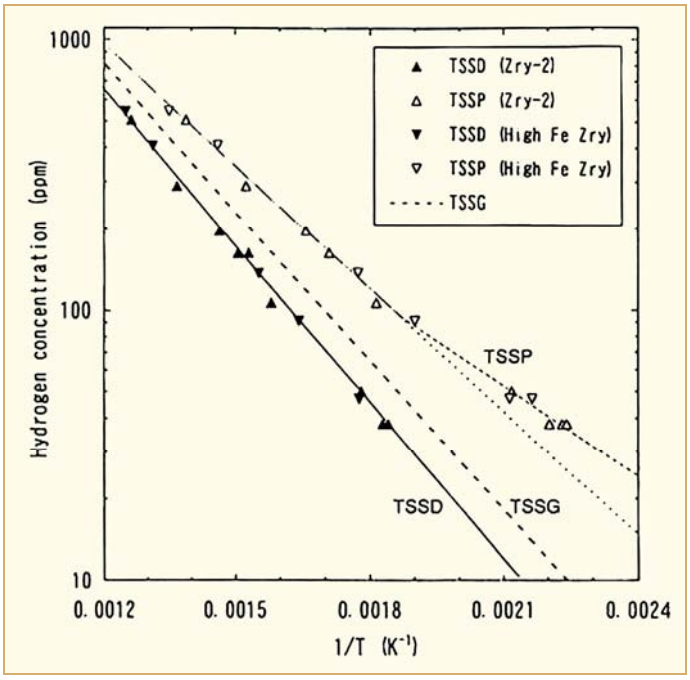

Figure 2-12: Solvi of TSS_D and TSS_P for Zircaloy-2 and high Fe Zircaloy, Une & Ishimoto, 2003.

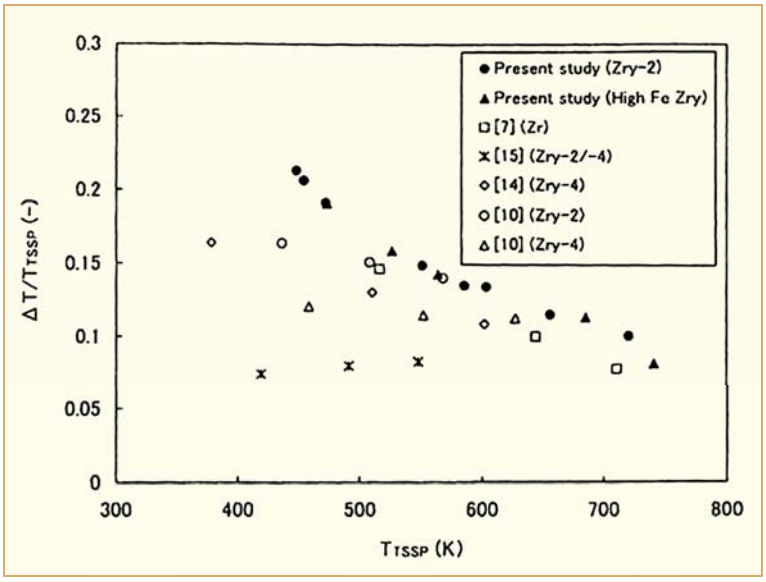

Figure 2-13: Thermal hysteresis as a function of TSS_P precipitation temperature, Une & Ishimoto, 2003.

In later work the authors compared the unirradiated high Fe Zircaloy-2 to pure Zr (Une & Ishimoto, 2004) and the results on Figure 2-14 show the similar hysteresis between dissolution and precipitation. In addition it further confirms the lower solubility of H in pure Zr compared to the Zircaloys, which can also be observed on Figure 2-9(b), Figure 2-10, and Figure 2-14. This may be due either to the difference in alloying content or the difference in O content; the higher O content of 1300-1500 ppm in the Zircaloys can increase their solubility for H as noted for "high O" materials in Figure 2-15. *This difference in solubility can be significant for the operation of Zr liners in BWR fuel, as discussed in Section 3.3.*

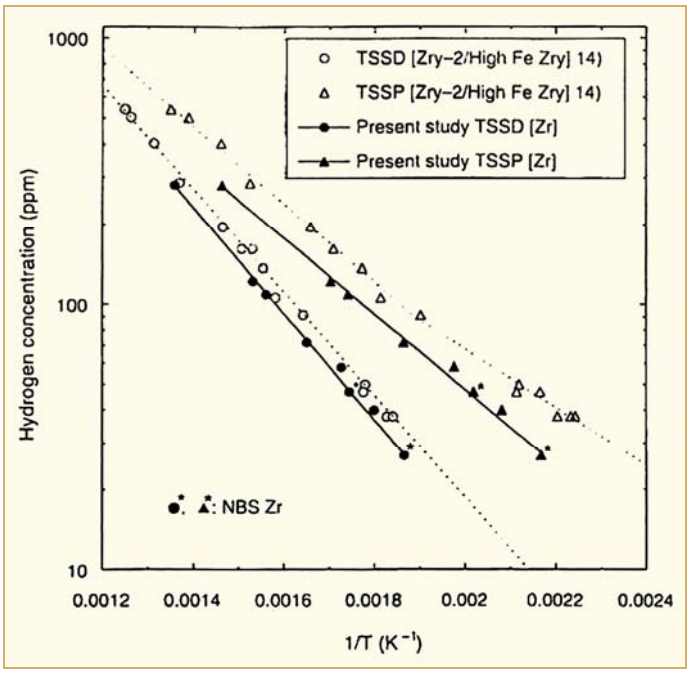

Figure 2-14: Comparison of TSS_D and TSS_P for unalloyed Zr vs. high Fe Zircaloy 2, Une & Ishimoto, 2004.

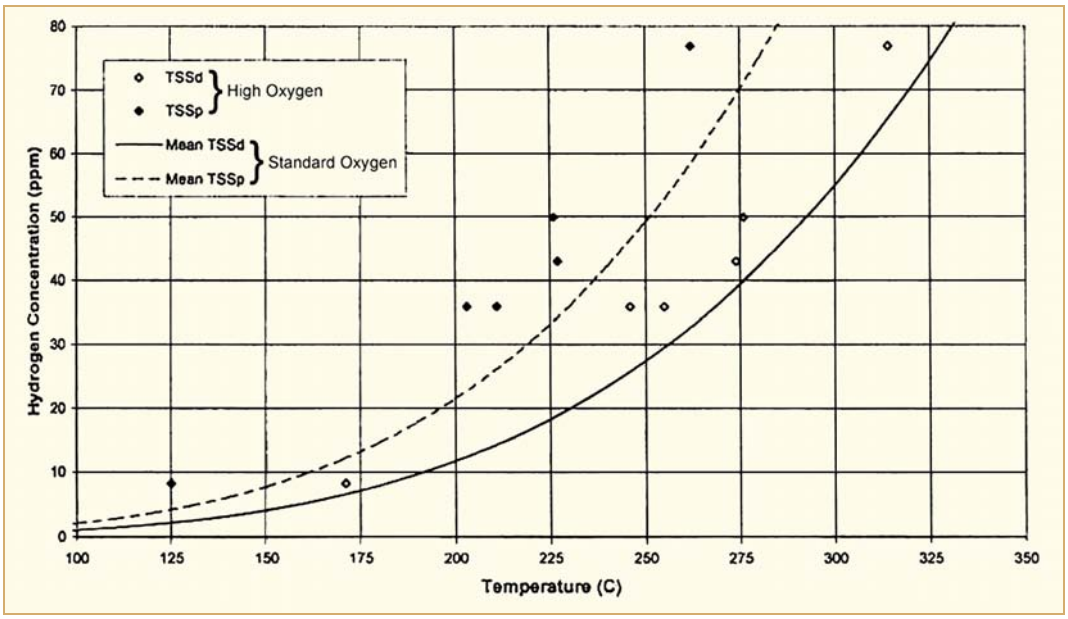

Figure 2-15: Comparison of *TSS* for standard and high oxygen Zircaloy-4, McMinn et al., 2000.

The effect of individual alloying elements on TSS_D of H in Zr was measured and compared to unalloyed Zr and various Fe level Zircaloy-2 materials, Setoyama et al., 2005. The results are shown on Figure 2-16. Binary additions of Ni and Cr to Zr had the most significant effect by increasing the H solubility, or *TSS*, while Fe and Sn had very little effect. Since the Ni can vary from 0.03 to 0.08% and Cr from 0.05 to 0.15%, the H solubility could vary slightly for Zircaloy-2 made to the same specifications.

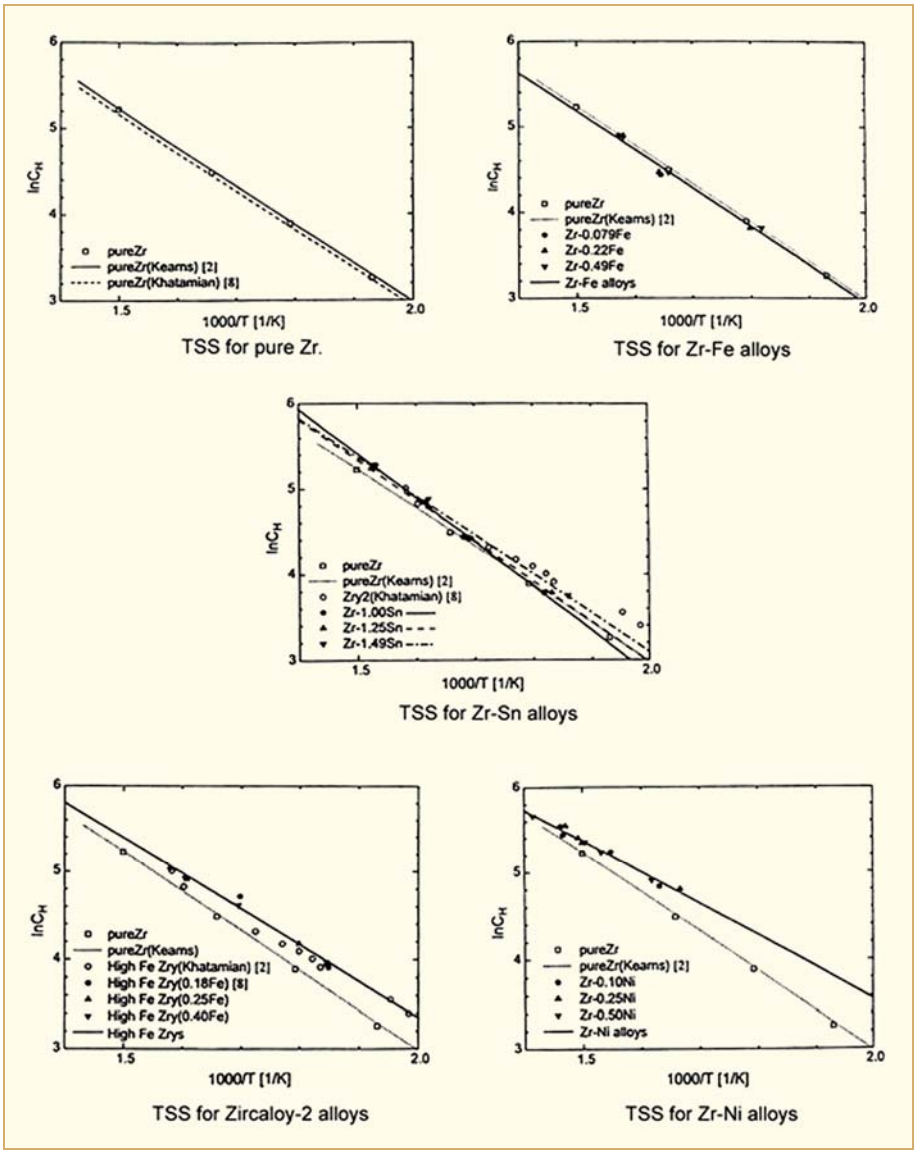

Figure 2-16: The effect of alloying elements on TSS_D of H in Zr, Setoyama et al., 2005.

Tests of Zircaloy-2 and -4 made by various processing methods appear to show the same *TSS* characteristics for all samples so that the Ni and Cr variations, within their specifications, fall within a small scatter-band, McMinn et al., 2000. The *TSS* curves, shown on Figure 2-17(a), include Zircaloy-2 and -4 Electron Beam welded (*EB*), Zircaloy-2 Pressure Tube (*PT*), Cold Worked (*CW*) at various levels (0% and 30%) and β quenched. These data could indicate a small increase in *TSS* in cold worked material. Trapping of hydrogen at dislocations during cooling has been observed, Roy, 1965.

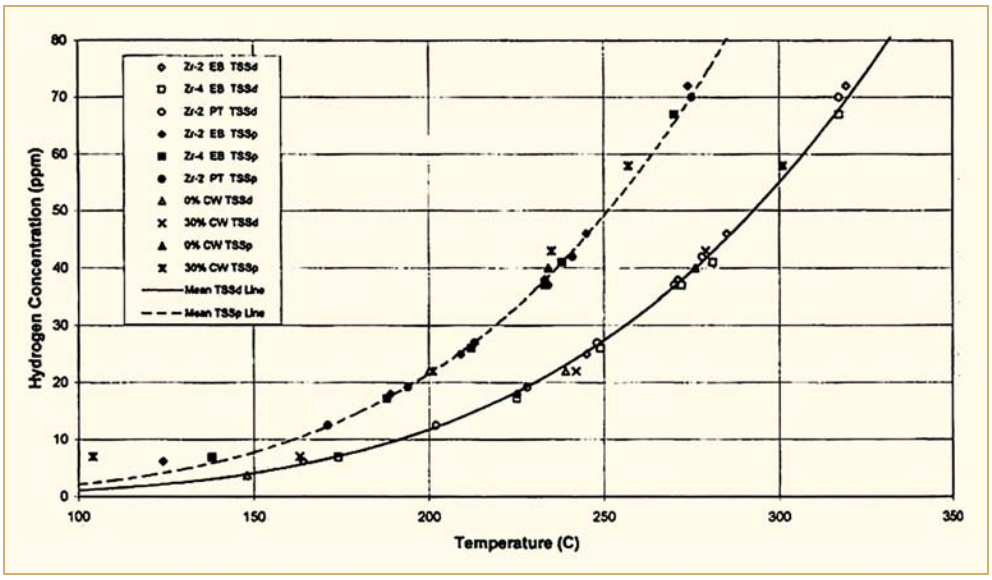

Figure 2-17(a): *TSS* data for unirradiated Zircaloy-2 and -4 made by various processes, McMinn et al., 2000.

Effect of stress

Data on the effect of stress on *TSS* are very limited and opinions on the effect of stress are a subject of controversy. Experiments on Zircaloy-4 specimens show that there is an effect, but it is much smaller than the effect of temperature, Kammenzind et al., 1998, Figure 2-17(b).

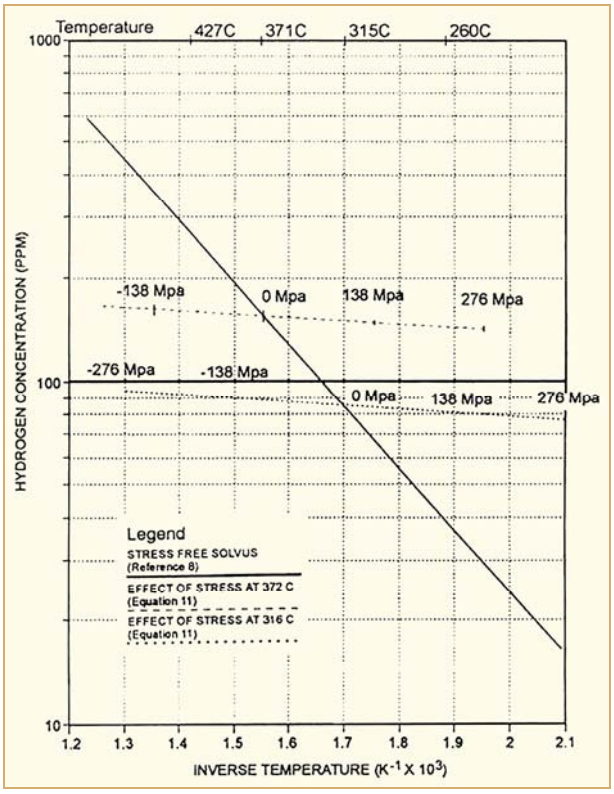

Figure 2-17(b): Hydride dissolution solvus, comparative effect of temperature and stress, Kammenzind et al., 1998.

On the other hand, a theoretical evaluation concludes that the effect of stress on *TSS* cannot be significant and that the determination of *TSS* on unstressed samples is reasonably valid, Puls et al., 2002. As reported in Cox & Rudling, 2000, hydrogen in solution in the α–Zr lattice occupies the tetrahedral interstices in the hexagonal α–Zr unit cell and causes a small dilation of the lattice, Martin & Rees, 1954. As a result of this, hydrogen shows a tendency to segregate to regions, such as the cores of dislocations, where the crystal lattice is already dilated, Cox, 1997. Because of this effect, hydrogen in solution in zirconium will migrate up a stress gradient (i.e. towards the region where the lattice is dilated by the elastic stress). Whether or not there is an effect of stress on the hydrogen solubility in Zr-alloys is determined by the difference between the lattice dilation caused by the hydrogen atoms in solution and the lattice dilation resulting from the formation of a second-phase hydride. These dilations can be described by the partial molar volumes of hydrogen in solution (V^h_H) and hydrogen in the appropriate hydride phase (V^h_{Hyd}) - usually δ–$ZrH_{1.66}$ - respectively. Measurements of these partial molar volumes have shown them to be nearly equal, so that the effect of external stress on *TSS* should be negligibly small, Coleman & Ambler, 1983, typically less than one centigrade degree. These effects of stress on hydrogen migration are critical to the mechanism of Delayed Hydride Cracking in Zr alloys, see Section 2.6 in the ZIRconium Alloy Technology (*ZIRAT13*)/ Information on Zirconium Alloys (*IZNA8*) Special Topic Report Entitled: "The Effect of Hydrogen on Zirconium Alloy Properties, Vol II". It should be noted that Kammenzind et al., 1998, do report a small effect of stress on solubility.

The effect of stress on *TSS* should not be confused with the effect of stress on re-orientation of hydrides during their precipitation, see Section 5.2 for more details.

Effect of irradiation

Using the *DSC* technique, two groups have recently provided data on the effect of irradiation on the solubility of hydrogen in recrystallized (*RXA*) or Stress Relief Annealed (*SRA)* Zircaloy-4, McMinn et al., 2000, and in *RXA* Zircaloy-4, Vizcaino et al., 2002, 2005 and 2007. Both obtained reasonable results for hydrogen solubility in unirradiated material, e.g. 200-250 ppm at 400°C (673K); 55-70 ppm at 300°C (513K). And both gave firm evidence that solubility is increased by irradiation. The effect of incremental fluence on solubility was not unambiguous. However, it does appear that the effect increases with increasing fluence in the range 1-10×10^{21} n/cm^2 E>1 MeV[1] for irradiation temperatures near 300°C (573K). McMinn et al. give an apparent solubility increase of about 25 ppm at 6-10×10^{21} n/cm^2, Figure 2-18, Figure 2-19 and Figure 2-20. Vizcaino et al. indicate an apparent increase of 100-200 ppm at 9×10^{21} n/cm^2. Follow-up work by Vizcaino et al., 2005 and 2007 using X-ray diffraction at room temperature indicate >40-80 ppm H is trapped by irradiation for material (same as earlier study) containing 180 ppm H. An example is given in Figure 2-21. It should be noted that "increase in solubility" really means increase in apparent solubility, as more than one solubility mechanism is likely operating.

Of particular importance is that the "increase in solubility" can be recovered by suitable post-irradiation thermal anneals. In the McMinn study, for material having a relatively low fluence (<5×10^{21} n/cm^2) partial recovery of solubility was obtained at 400°C (673K) for 1 hour, and full recovery at 500°C (773K) for 1 hour. For high fluence material (1×10^{22} n/cm^2) only 60% recovery was obtained at 500°C for 1 hour.

In the Vizcaino et al. studies, the recovery results were varied. Some recovery was observed at <380°C (653K) for 10 minutes in most materials. It appears that for low fluence, <5×10^{21} n/cm^2, E>1 MeV, annealing in the range 500-611°C (773-884K) recovers most the solubility change. For high fluence material, >5×10^{21} n/cm^2, annealing in the range 500-611°C (773-884K) recovers only part of the solubility change.

[1] 1×10^{21} n/cm^2 corresponds to a burnup of about 5 MWd/kgU.

From the data discussed above, it can be concluded that hydrogen exists in three forms in irradiated Zircaloy: 1) soluble hydrogen, 2) hydrides, and 3) hydrogen trapped by irradiation produced defects. The latter can be released by post-irradiation annealing. These phenomena are related to formation and annealing of radiation damage of various types. The most probable are <a> component dislocation loops which form at low fluence and are thermally stable up to about 400°C, and <c> component dislocation loops which form at intermediate fluences (greater than about 5×10^{21} n/cm^2, E>1 MeV) and are stable until higher than 600°C. Full details can be found in Adamson, 2006.

One recent study, Ogata et al., 2007(b), gave results that did not support an irradiation effect on hydrogen solubility. These authors also used the *DSC* method and obtained reasonable results for unirradiated material. Using high fluence Zircaloy-2 barrier cladding, they found no difference compared to unirradiated controls, except for perhaps a small increase at <250°C. It is speculated that irradiation damage annealing might have occurred during testing or that non-uniform hydride distribution could perturb results; however the experiment was carefully conducted so further consideration must be given.

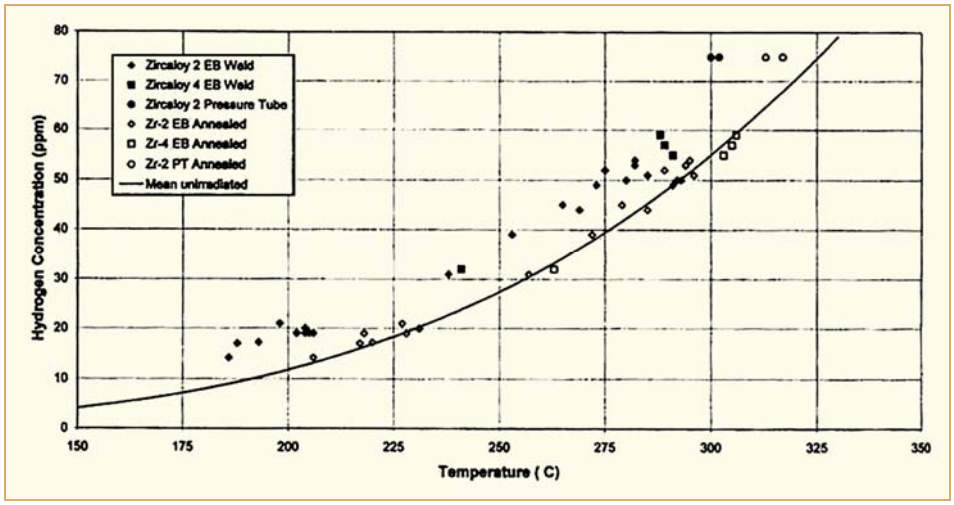

Figure 2-18: TSS_D for irradiated and post-irradiation annealed Zircaloy samples compared to the unirradiated mean line, McMinn et al., 2000.

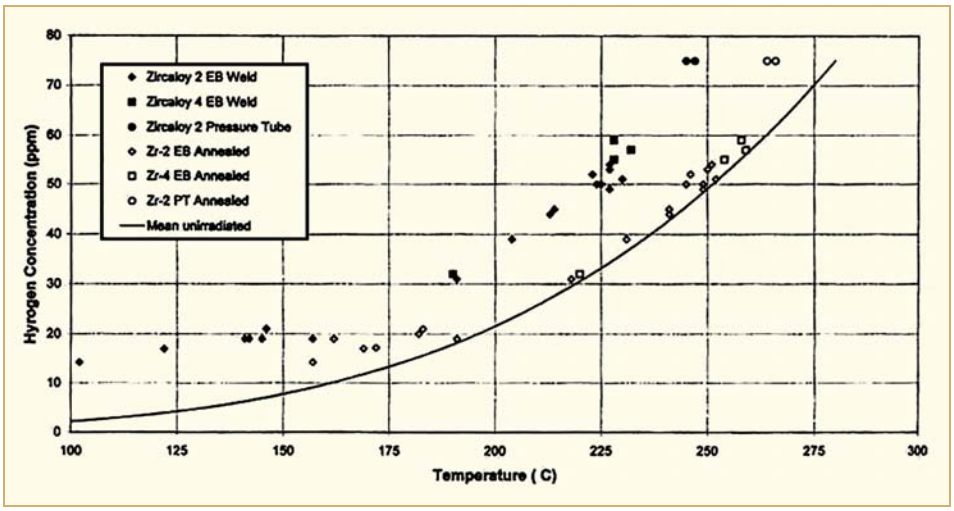

Figure 2-19: TSS_P for irradiated and post-irradiation annealed Zircaloy samples compared to the unirradiated mean line, McMinn et al., 2000.

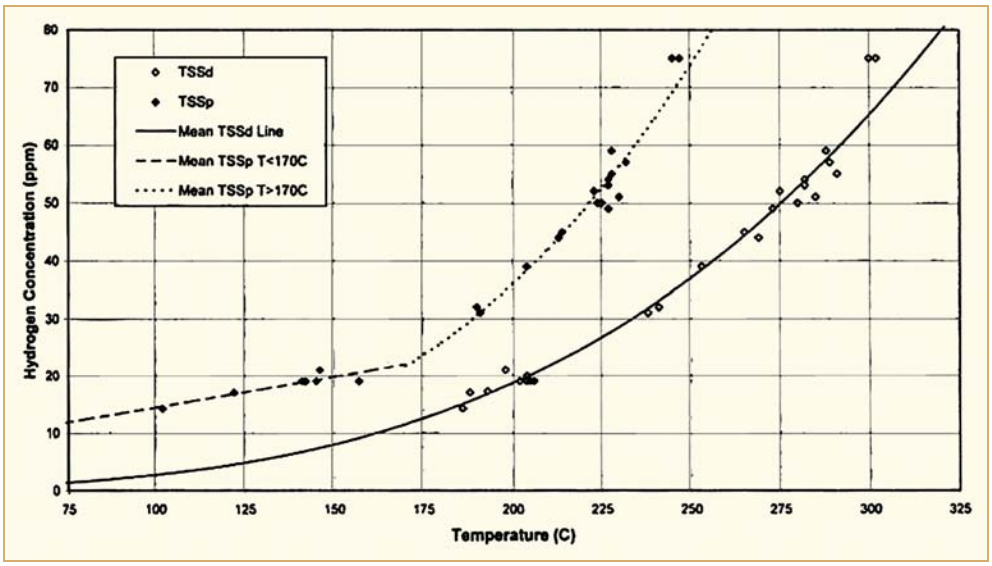

Figure 2-20: *TSS* data for irradiated Zircaloy-4, McMinn et al., 2000.

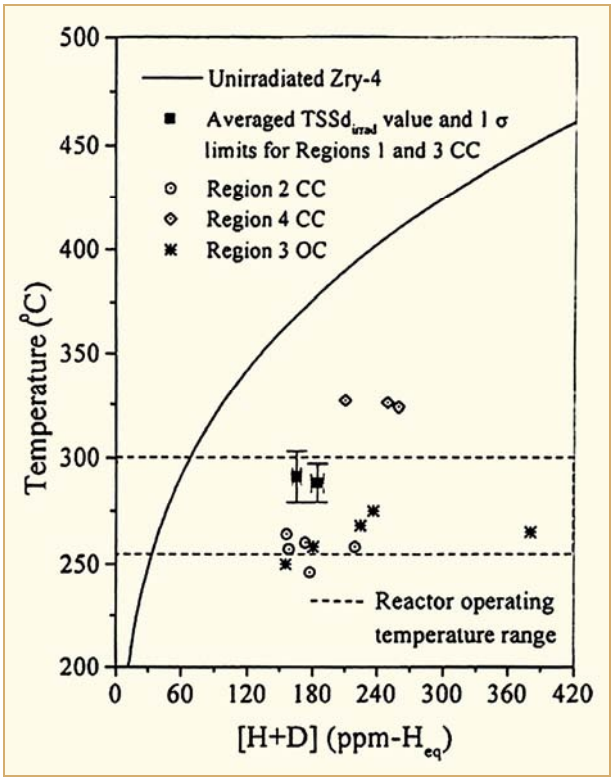

Figure 2-21: TSS_D first run values averaged for regions 1 (<0.05x10^{22} n/cm^2), and 3 CC (1x10^{22} n/cm^2). The solid line corresponds to unirradiated fully recrystallized Zircaloy-4, Vizcaino et al., 2002.

Precipitation of hydrides at a lower temperature in irradiated materials is advantageous to dry storage conditions, at which time the internal gas pressure and the resulting clad stresses will be lower benefiting the creep stresses and the stress levels for hydride re-orientation.

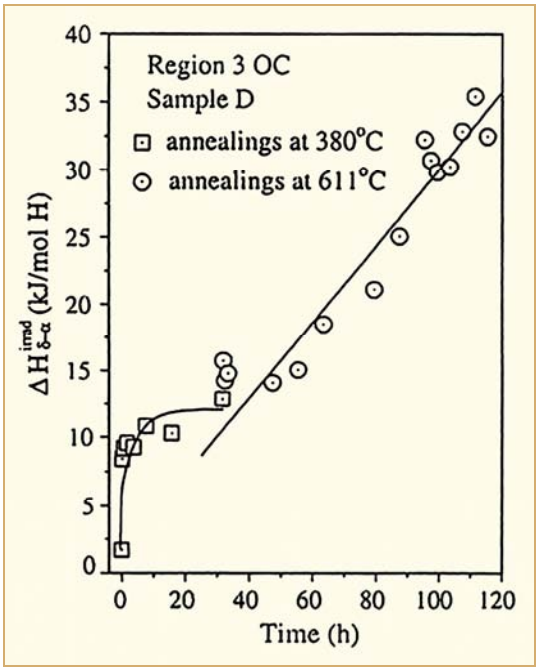

Figure 2-22: Enthalpy evolution with long thermal annealings of irradiated Zircaloy-4. ΔH for unirradiated material is about 38 on given scale, Vizcaino et al., 2005.

Summary of effects that influence hydride dissolution and precipitation

The data discussed in this section indicate the parameters that influence H solubility and precipitation in Zr and its alloys and these are summarized below (these do not apply to re-orientation of hydrides):

- Increasing O in solid solution decreases the solubility in the β phase and may or may not increase it in the α phase.
- Increasing Ni and Cr alloying elements increase the solubility.
- Pure, low oxygen Zr has a lower solubility for H than the Zircaloys with 1000-1500 ppm O.
- Irradiation increases the solubility.
- Thermal cycling appears to be able to increase solubility.

The following parameters do not appear to have a significant effect the H solubility:

- Increasing Fe and Sn alloying elements.
- Differences between Zircaloy-2, Zircaloy-4 and Zr- 2.5 Nb of the same microstructures.
- Grain size.
- Heating and cooling rates.
- Stress, although this is controversial.

2.2.2 Diffusion

As noted in the previous section, the solubility of H in Zr and its alloys is extremely low at low temperatures and increases at higher temperatures. The diffusion of H in solution at the higher temperatures is quite rapid. The *diffusion coefficient* is given by:

$$D = D_{\circ} \exp(-Q^{*}/RT)$$

where D = diffusion coefficient, or diffusivity, in cm^2/sec
$D_{\circ}$ = limiting diffusion coefficient at unlimited temperature
Q^{*} = activation energy for diffusion, or heat of transport in cal/mole (typically 6000 cal/mole)
T = absolute temperature in K

The diffusion coefficient as a function of temperature for pure Zr and Zircaloys is given on Figure 2-23. Data at temperatures as low as 150°C can be found in Cox & Rudling, 2000 or Cupp & Flubacher, 1962.

Data that show higher diffusion coefficients in the β phase and in the δ hydride phase are summarized on Figure 2-24; these are significant in structures that stabilize these phases.

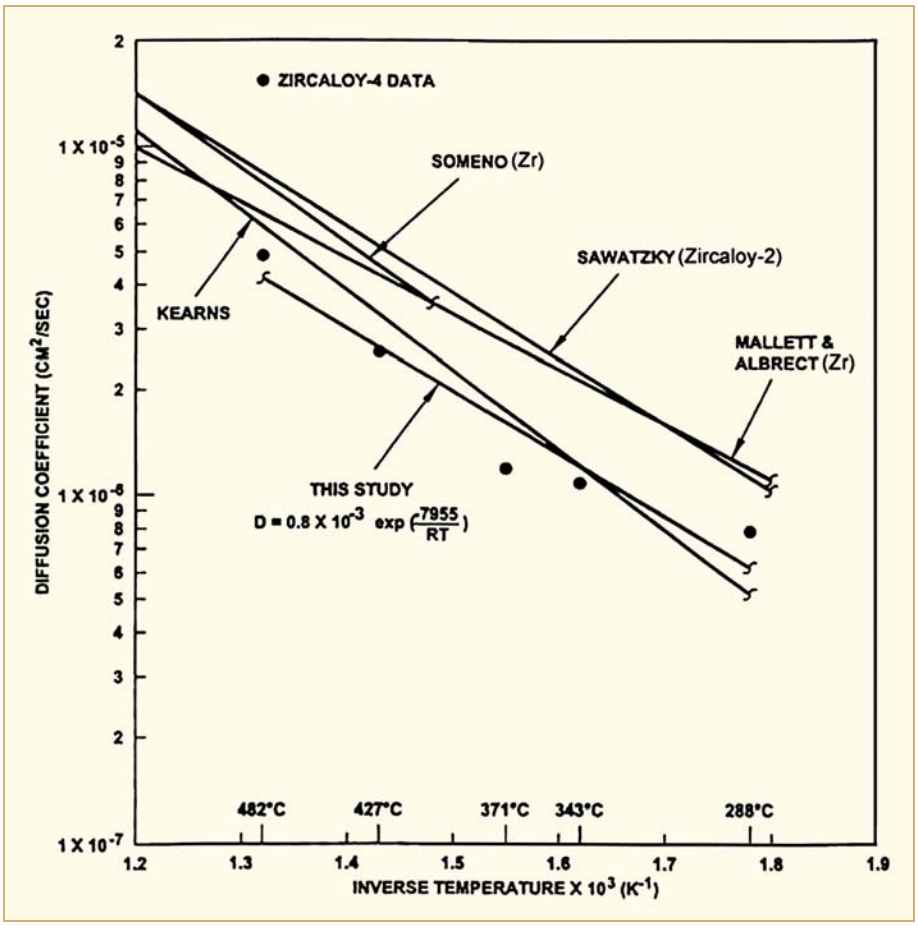

Figure 2-23: Diffusion coefficients of H in alpha Zr and Zircaloys, Kammenzind et al., 1996.

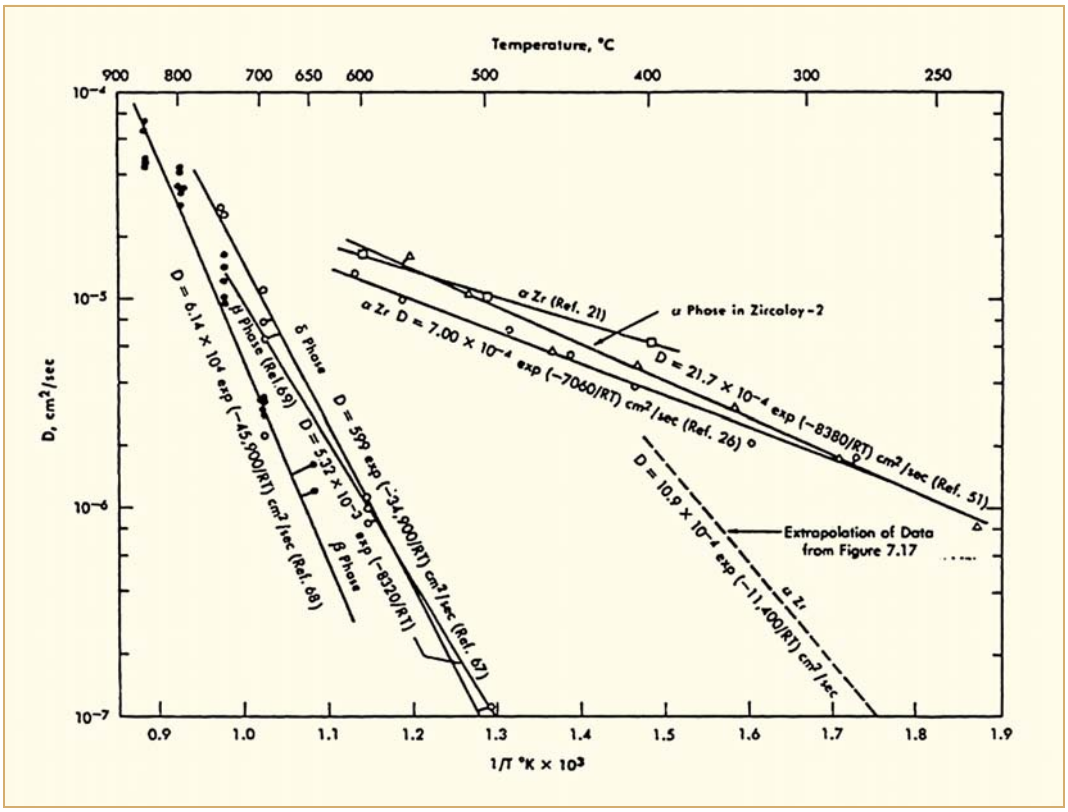

Figure 2-24: Diffusion of H in alpha and beta phases of Zr, Mueller et al., 1968.

As an example, using a diffusion coefficient of 1.5×10^{-6} cm²/s at 310°C, the time required for complete H diffusion across a concentration gradient can be calculated to be, t(time)=x^2(distance)/D, 1.8 hours over a distance of 1 mm. This represents a very short time for diffusion across the distance equivalent to a cladding wall thickness.

The *heat of solution*, the difference in molar free energy of hydrogen in the metal and in the gas phase, increases with decreasing temperatures and this causes the H to diffuse down a temperature gradient or a concentration gradient, a significant effect at fuel operating conditions. The diffusion of H in Zr is defined as:

$$J = -D\Delta C - \frac{DQ^* C \Delta T}{RT^2}$$

where J = H atom flux in the metal
D = diffusion coefficient for H as defined above
C = total local H concentration
Δ = rate of change in C or T
Q^* = heat of transport (generally around 6 Kcal/mole)

This relationship will predict rapid diffusion of H either down a temperature or a concentration gradient, but this high rate will only occur if the concentration in colder end of the temperature gradient is above the solubility limit and will form hydrides.

While the ΔC term tends to satisfy the hydrogen concentration differential, one can frequently observe that in response to a temperature gradient the ΔT term can overcome the ΔC term to produce a relatively high H concentration in the coolest region of the Zr component. The H can diffuse down a temperature gradient even if it requires diffusion up the concentration gradient, or vice versa, depending on the operating conditions.

3 Hydrogen pickup during corrosion

3.1 Mechanisms

A part of the hydrogen formed by the aqueous corrosion of Zr-alloys is absorbed by the metal. The H content of the structural materials and its effects on their mechanical properties and dimensional behaviour is important, since the integrity of the fuel assembly can depend on them.

The absorption of H by Zr and its alloys is the result of the corrosion reaction at operating temperatures:

$$Zr + 2H_2O \rightarrow ZrO_2 + 2H_2$$

Only a fraction of the H produced is absorbed by the Zr metal and the "hydrogen pickup fraction" or "percentage hydrogen uptake" is defined as the ratio of H entering the metal to that formed by the corrosion reaction during the same period. The H that is absorbed by the metal does so as an integral part of the reaction of Zr with the water molecule rather than by the reaction with any dissolved H in the water, except at high H pressures beyond any operating conditions in Light Water Reactor (*LWR*s), such as H/O ratios of 10^3 since H penetration through the essentially ever present oxide layer is slow, Cox & Johnston, 1962 and IAEA TECDOC-996, 1998. A H take up from the coolant can also occur in Ni containing alloys if the corrosion potential is so low that Ni remains metallic in the oxide. Ni can take up dissolved H catalytically.

The corrosion process consists of an anodic half-cell reaction at the metal-oxide ($Zr\text{-}ZrO_2$) interface to form the oxide and make the oxide film thickness grow [$Zr+2O^{2-} \rightarrow ZrO_2+4e^-+2$], and a cathodic half-cell reaction at the oxide-coolant interface to form H [$2+2H_2O+4e^- \rightarrow 2O^{2-}+4H^+$]. The cathodic reaction is between an oxygen atom vacancy [$2\square^{\circ}$] and a water molecule on the oxide surface, giving an oxygen ion, filling the vacancy, and producing two protons. Two electrons from the oxidation of the Zr metal atom then discharge the protons to give two H atoms at the free surface. A fraction of these atoms then enter the metal and the remaining atoms recombine with the water coolant. The means by which the H then enters the metal is the topic of numerous theories, but no resolution, Cox, 1997.

Various theories proposed for the transport of H into the metal have been:

- H diffuses through flaws in the impervious, or porous oxide film, since reliable diffusion measurements of H through the solid oxide itself are not available.
- H diffuses through thin oxide films after all.
- H diffuses through a group of *SPP*s that bridge the oxide film, a function of their composition, size and distribution of the *SPP*s in the oxide film.
- Proton conduction across a thin oxide film by OH^- concentrated in the lattice distortions of the oxide.

Details of these proposed mechanisms, none of which have been confirmed, are discussed by Cox, 1999.

Factors that affect the amount of hydrogen pickup include:

- Oxide film characteristics, such as thickness, morphology, and crystal structure.
- *SPP*s of various characteristics and potentially other compounds in the oxide film.
- Metal alloy composition and microstructure.
- Water chemistry and radiolysis of the water.

3.2 Ex-reactor results

3.2.1 Introduction

Ex-reactor corrosion tests are often used for H pickup studies, and they can be useful for screening purposes. The most meaningful data, however, are the evaluations of in-reactor experience and analyses of materials irradiated under prototypical operating conditions.

The fraction of corrosion hydrogen, that is picked up, changes slightly over the time of corrosion exposure (e.g. before and after transition), e.g. Harada & Wakamatsu, 2007. For practical data analysis and for design purposes an average constant value measured at long exposure times is usually applied.

3.2.2 Effect of alloying elements

Early ex-reactor autoclave tests were used to evaluate the effect of various potential alloying elements in Zr on H pickup (e.g. Figure 3-1, Figure 3-2 and Figure 3-3). Whereas tin - being in solid solution within the metal matrix - was found to have little effect on the Hydrogen PickUp Fraction (*HPUF*), the presence of nickel - contained in *SPP* - had a pronounced effect on *HPUF*. V, Cr - contained in *SPP* -, and Nb –to a large extent (0.5%) in solid solution - reduce the *HPUF*. The beneficial effect of Nb is explained by the observed surface segregation of Nb^{5+}, which should enhance the cathodic water reduction, Bossis et al., 2002 and Ramasubramanian et al., 2002.

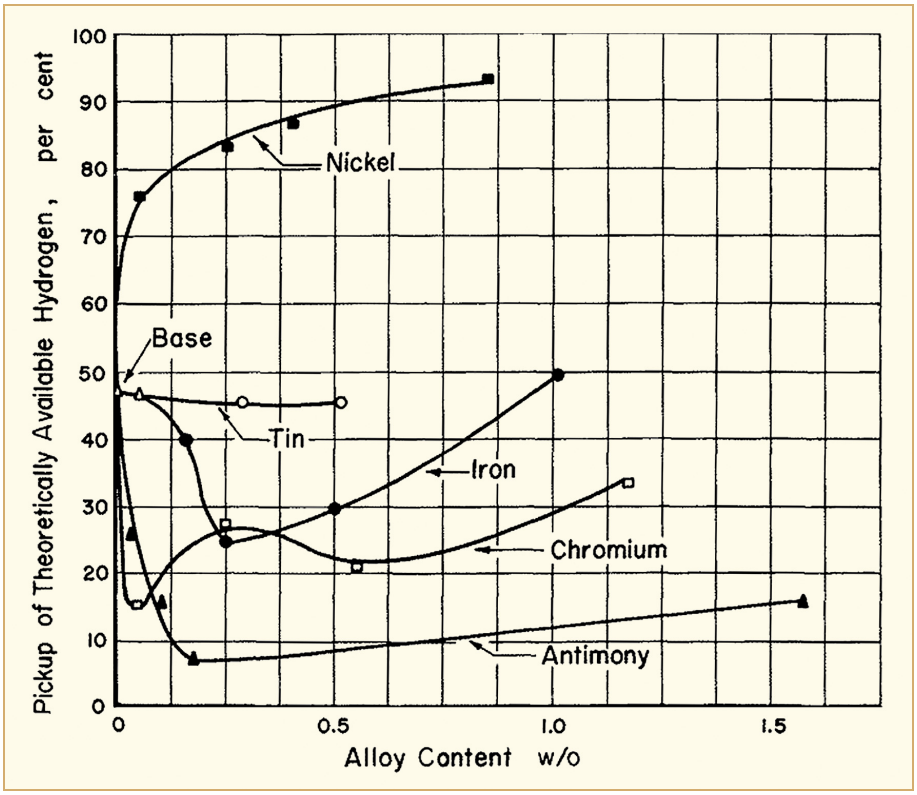

Figure 3-1: Hydrogen pickup in different Zr alloys exposed in 650°F (343°C) degassed water under static conditions for 575 days, Berry et al., 1961.

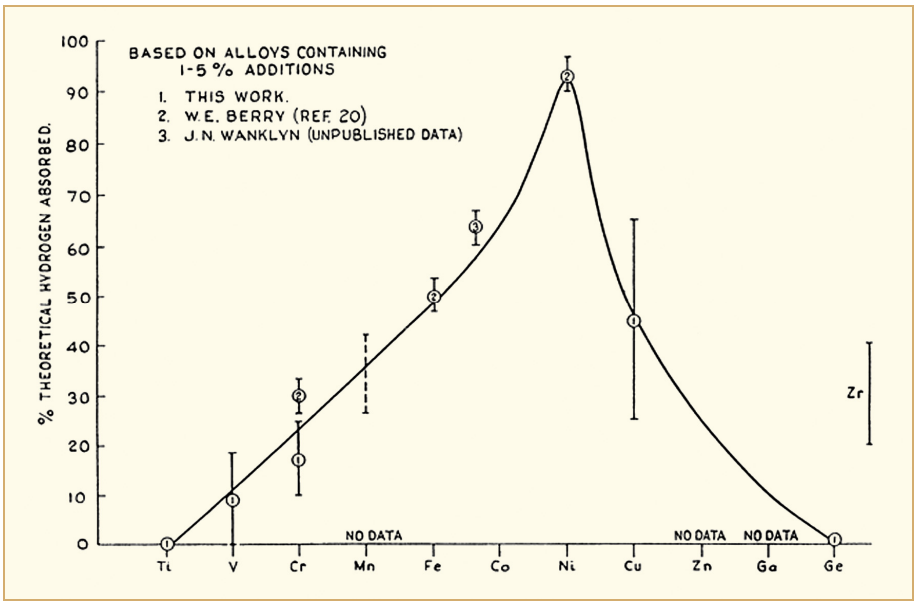

Figure 3-2: Effect of some alloying elements forming intermetallic precipitates on hydrogen uptake percentage, Cox, 1976.

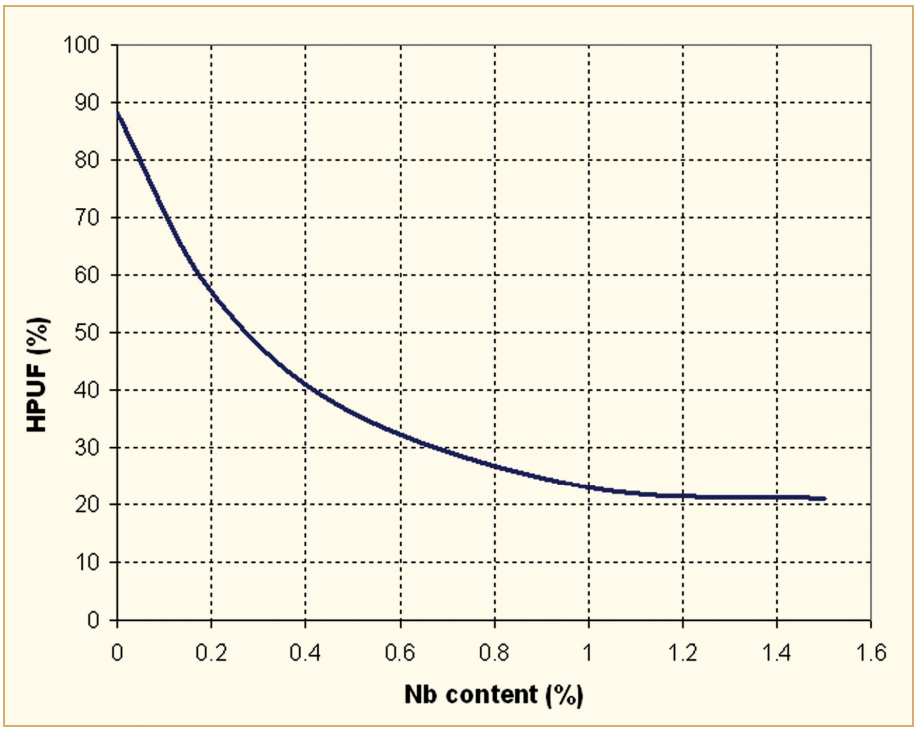

Figure 3-3: Effect of Niobium on the hydrogen pickup fraction of binary Zr-Nb alloys degassed water under static conditions at 350°C after 750 days, Kiselev et al., 1962.

4 Hydride distribution

4.1 Introduction

At the operating temperature, the zirconium cladding is expected to absorb hydrogen (H). The H that is in solution in the Zr alloy components can diffuse and distribute or redistribute itself creating localized concentrations of hydrides. Hydrides formed by H levels above the *TSS* will remain relatively stable. The distribution of H is controlled primarily by the following factors:

- Ingress rates.
- Temperature gradient.
- Solubility in the alloys the H is diffusing through during heating and cooling cycles.
- Cooling rate and number of cooling cycles.

These factors are interactive as discussed before and, depending on the materials and the operating conditions, some factors may dominate over the others.

The cladding is obviously the subject of most of the redistribution events, due to the variety of temperature gradients present. Non-heat generating structural components (if γ heating is neglected) will have uniform distribution of hydrides, unless some special circumstances exist among the factors mentioned, such as welded sections. The redistribution events for unfailed cladding are discussed first for *monotube cladding* that is cladding made of one material, and second for *duplex cladding* that has a thin corrosion resistant outer layer, for *PWR*s, and a thin Pellet Cladding Interaction (*PCI*) resistant inner layer, for *BWR*s.

The presence of H, in the form of water molecules, in the oxide layer should be noted. While this is unlikely to affect the H content, distribution, or redistribution in the cladding, it can affect the experimental results to determine the total H content in the cladding if the oxide layer is not removed prior to analyses. Any evaluation of experimental data should review this aspect of the examination procedures. The amount of H in the oxide layer can be considerable as identified by Bettis Labs., (Kammenzind et al., 1996) and Paul Schrerrer Institute (*PSI*) (Goll & Hoffmann, 2002). The Bettis data showed little difference in H content between unirradiated samples with and without the oxide layer; however, samples irradiated to 10^{22} n/cm^2 (E>1 MeV) with oxide films up to 100 μm had 400-2300 ppm H in the oxide.

4.2 Mechanistic aspects

If the rate of H_2 absorption is below a critical ingress rate, the effects of local variations in solubility are sufficient to prevent precipitation of a solid hydride rim at the surface of ingress. Figure 4-1 shows this critical ingress rate versus temperature based on different corrosion tests in LiOH solutions. Solid hydride layers are formed in tests under (1) gaseous hydriding, (2) cathodic hydrogen uptake and (3) fast corrosion in LiOH-water mixtures especially at low temperatures when hydrogen diffusion is low. In reactor such a surface hydride rim due to a high ingress rate only forms under abnormal conditions, as in the case of fuel failures or surface contaminations with metallic Ni, e.g. Cox & Ling, 1979.

The heat flux through the cladding creates a radial ΔT across the cladding wall with the lower temperature at the Outer Diameter (*OD*) in contact with the coolant. The increasing heat of solution with decreasing temperature (see Section 2.2.2) causes the H concentration in solution to be slightly higher at the colder surface. The relationship of the *TSS* to the H distribution is shown on Figure 4-2. The *TSS* will be reached first at the colder surface and thus all the H absorbed above the *TSS* will precipitate at this surface. Under normal conditions this will be a two phase, $\alpha+\delta$, structure.

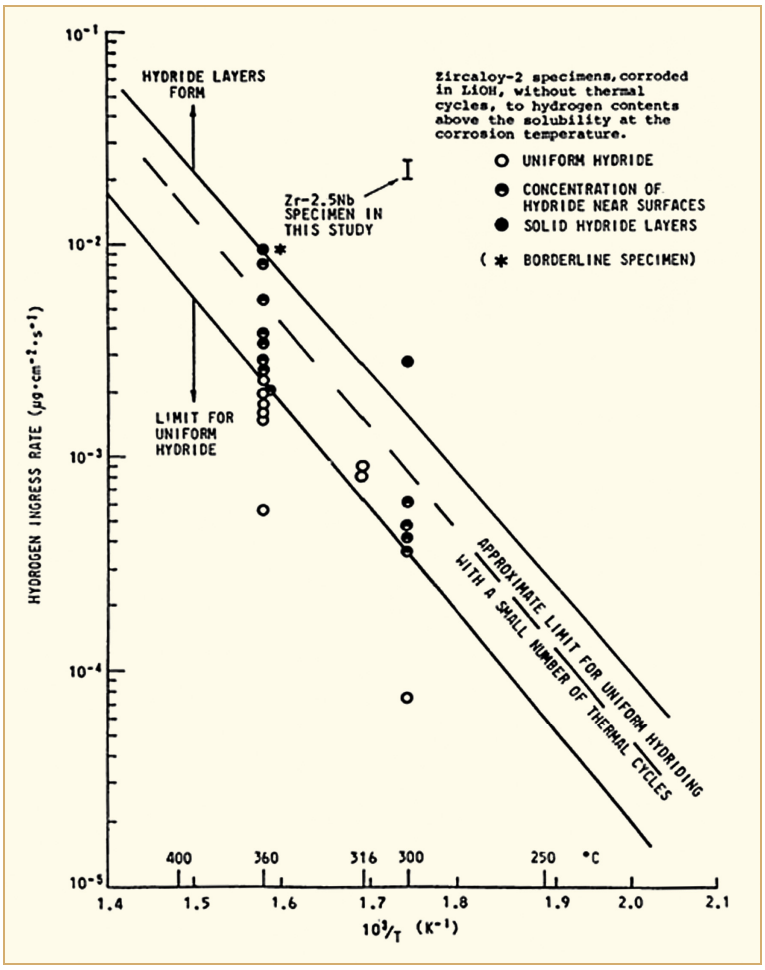

Figure 4-1: Critical hydrogen ingress rate for surface hydride layer formation, Cox & Ling, 1979.

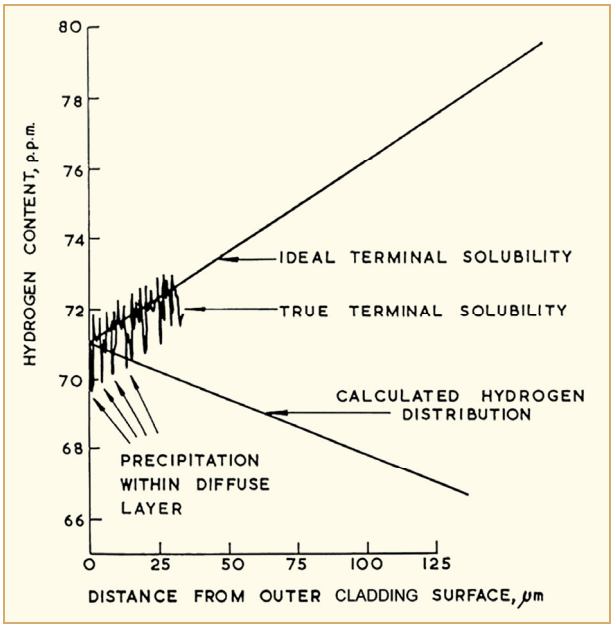

Figure 4-2: The effect of the temperature dependent *TSS* on hydrogen distribution in cladding wall, Asher & Trowse, 1970.

Figure 4-3 shows the increasing H content toward the *OD*. This structure will be similar along the longitudinal axis of the cladding with variations in total H due to the increasing temperatures toward the top of *PWR* fuel rods. At cooler spots on the clad generated by pellet-pellet gaps or spalled cladding, discussed next, the region could consist of solid hydrides.

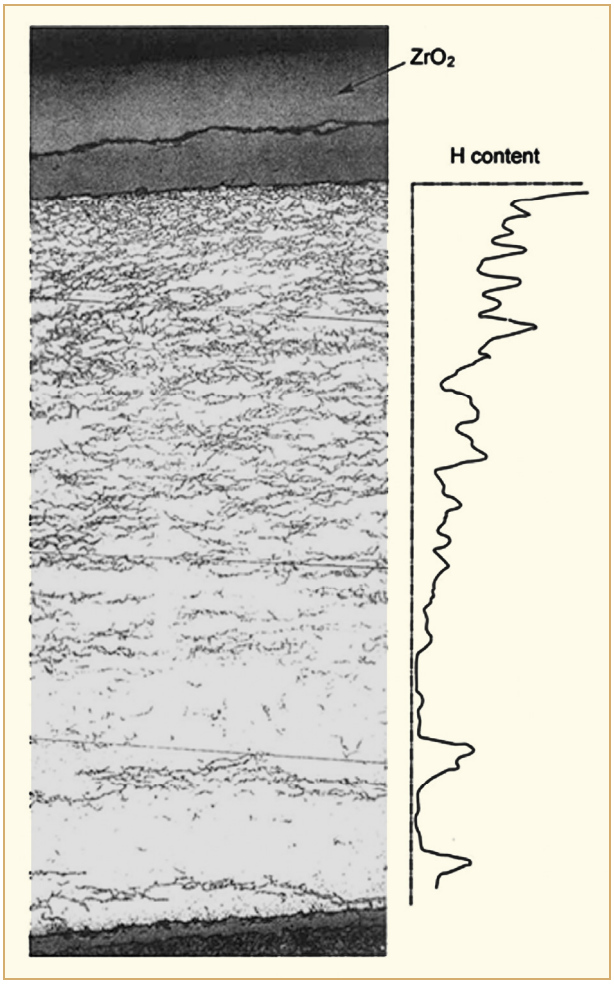

Figure 4-3: Through-thickness distribution in stress-relieved Zircaloy-4 cladding irradiated for 5 annual cycles in a *PWR*, , Guedeney et al., 1991.

Circumferential hydride concentration gradients have been observed on fuel rods. These are attributed either to:

- Circumferential differences in corrosion and hydrogen pickup rate or
- circumferential H diffusion down thermal gradients established by variations in oxide thickness and their thermal resistance that cause variations in the oxide metal interface temperature around the rod circumference.

5 Hydride orientation

5.1 Introduction

The orientation of the hydride platelets that form during normal reactor operation, as described in Section 4, have usually an axial-circumferential orientation, Figure 5-9, in tubes (and axial-tangential orientation in strips) and this hydride orientation remain during wet storage of the spent fuel.

However, the hydrides can become oriented in the axial - radial direction if they precipitate during operation under high tensile stresses, e.g. from fuel swelling, or precipitate from solid solution during cooling under a tensile hoop stress.

Reorientation could occur during reactor operation during cool-down or power cycling, although it is generally unlikely. But, it can also occur during cooling under dry storage conditions provided that:

- The hydrogen content is large enough and,
- the tensile hoop stresses are large enough

However, only the hydrogen in solution may reorient during cooling while the hydrides existing before cooling will remain in their original circumferential orientation.

In summary the factors that affect hydride re-orientation in irradiated cladding are:

- Hoop tensile stress level.
- Maximum temperature.
- Cool-down rate and final cool-down temperature.
- Solubility of H in the specific alloy at its specific burnup that will determine the amount of H in solution at the max. temperature and the amount of circumferential hydrides.
- Microstructure features such as grain size and shape, amount of cold work, dislocation structures and perhaps others.
- Texture
- Time

The radial hydrides visible in metallographic cross sections can be present in a wide variety of sizes and distributions as well as fractions of the total hydrides present.

Radial hydrides in zirconium alloy cladding are undesirable because they reduce the cladding ductility during handling or transportation. For this reason considerable attention and effort is spent to define the conditions for radial hydride reorientation and evaluate its effect on mechanical properties (see Section 8) and the performance of the fuel, particularly during hypothetical accidents. One of the objectives of the dry storage regulations in the US is to define the conditions to limit the hydride reorientation tendency during dry storage.

The undesirable effect of radial hydrides was recognized already at the beginnings of the nuclear Zr industry in the early 60s. Extensive work was done, much of it in Canada at Atomic Energy of Canada Limited (*AECL*), to study the factors that form radial hydrides and establish fabrication procedures that would provide plates and tubing with textures that avoid the formation of radial hydrides in the as-fabricated state. The current 30° texture for tubing used by most vendors is a result of that effort. A good review of that work is given in Douglass, 1971 and Ells, 1968.

Some of the most recent work in trying to identify the parameters that control radial hydride formation and their effects on mechanical properties is described in this Section and Section 8. The evaluation and application of these data must consider whether the test conditions adequately represent the event they are supposed to simulate. For example, the time-temperature history for reorientation will be different for simulating a reactor shutdown, vacuum drying prior to dry storage, or the subsequent dry storage conditions. The levels of H and microstructure features will vary from one material to the other. The effects of radiation could be partially or completely annealed out by sufficiently high temperature histories.

The mechanical test method itself should represent the stress distribution expected in the component; for the cladding, the tests that produce biaxial stresses best represent the internal pressure generated hoop stresses. Hydride orientation does not have much effect on tensile strength or ductility of tubes with radial hydrides at either 20° or 300°C if the stress is applied in the axial direction of the tube. A significant reduction in ductility occurs at 20°C, however, if the stress is applied to the same material in the circumferential direction with the stress perpendicular to the plane of the hydride platelets.

The majority of the tests have been made on pre-hydrided, unirradiated materials for reasons of cost and convenience and these are adequate for some applications. The difficulty of hydriding unirradiated materials to produce the hydride structure that simulates the irradiated material should not be underestimated. The number of tests of irradiated materials is increasing as materials and funding became available.

The effect of hydrides on mechanical properties of Zr alloys is described in Section 8.

The mechanistic aspects and parameters important for hydride orientation and reorientation are described first. The current view of the Nuclear Regulatory Commission (*NRC*) of the effects of radial hydrides and their effect on regulations is described next. The major concern of the *NRC* is the effect of radial hydrides during dry storage, specifically during handling and design base transportation accidents. Finally the available information on hydride orientation and reorientation are summarized in detail for:

- Recrystallised (*RX*) Zircaloy-2.
- Cold Work and Stress Relieved (*CWSR*) Zircaloy-4, and
- the Zr-alloys, with improved corrosion resistance, used for modern *PWR* fuel elements and the Zr2.5Nb alloy applied for the *CANDU* pressure tubes.

5.2 Mechanistic aspects and parameters important for hydride orientation and reorientation

The hydride orientation is usually described via the hydride orientation factor, the number of hydrides in an angular range between 90° and a reference angle (e.g. 45%) divided by the total number of hydrides.

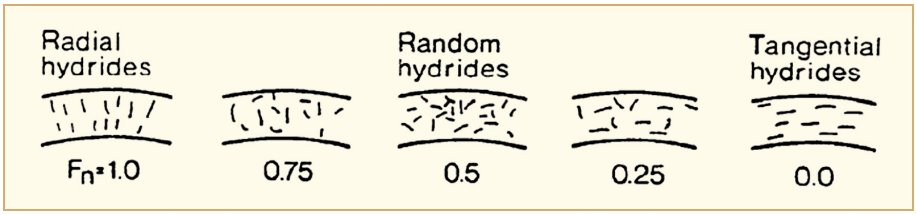

Figure 5-1: Typical hydride orientation observed in metallographic cross sections of Zr-alloy claddings, Källström, 1975.

Hydrides have a larger volume than Zr metal, e.g. the δ-hydride by about 16%. Thus a large strain energy is connected with the nucleation of hydrides. Precipitate nucleation in solids under such conditions is always heterogeneous. Non-equilibrium defects such as excess vacancies, dislocations, grain boundaries and free surfaces increase the free energy of the material and are the preferable sites for hydride nucleation. The exact hydride precipitation process is still being examined. According to recent examinations, Zhao et al., 2007, it probably consists initially if nucleation and growth of a metastable hexagonal ζ-hydride (Zr_2H, ζ-hydride needles with a length of <500 nm) which transforms to the stable fcc δ-hydride ($ZrH_{1.6}$), or under fast cooling rates to a metastable fct γ-hydride (ZrH). In fuel components the δ-hydride is the preferential Zr-hydride.

Applying *TEM* examinations, often three different hydride morphologies are distinguished:

1) Intra-granular hydride needles (0.1-1 μm in length), see Figure 5-2.
2) Inter-granular hydride platelets (1-5 μm in length, parallel or perpendicular to the grain boundaries), see Figure 5-3.
3) Trans-granular hydrides running across several α-Zr grains, see Figure 5-4.

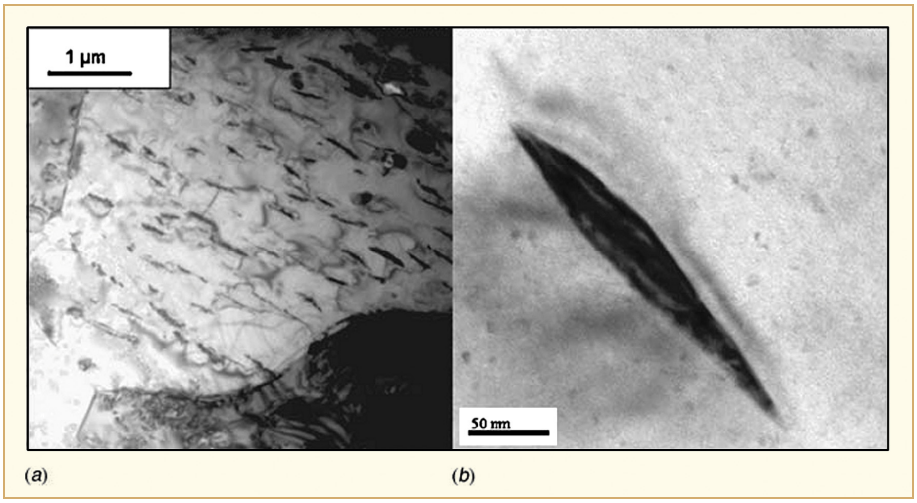

Figure 5-2: (a) Needle-like intra-granular hydrides formed after water quenching. (b) Focusing on a typical small hydride having a sharp interface, Zhao et al., 2007.

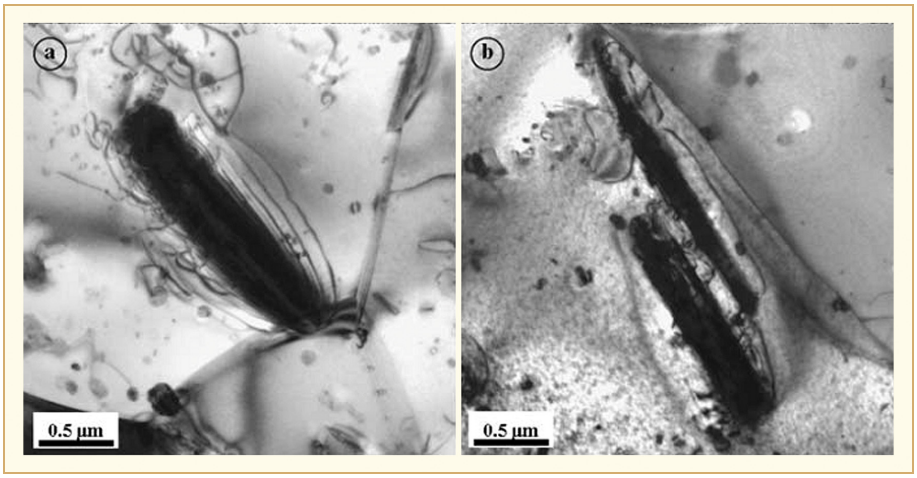

Figure 5-3: Inter-granular hydrides in a furnace cooled samples. (a) A hydride precipitated almost perpendicular to a grain boundary; (b) A hydride precipitated along the grain boundary, Zhao et al., 2007.

6 Effect of a cladding Outer Diameter (*OD*) hydride rim on corrosion

6.1 Introduction

This topic became of interest in the last two decades when *PWR* fuel was exposed under high power to high burnup and developed hydride rims on their *OD* exposed to the coolant.

6.2 Ex-reactor data

The water corrosion of Zr hydrides was recognized to be higher than that of Zircaloys, by ex-reactor tests on solid hydrides some time ago, Cox & Johnston, 1962.

A possible acceleration of corrosion when hydrides precipitate at the metal oxide interface was discussed controversially in the early sixties, e.g. Cox & Johnston, 1962. In 1990, Garde, 1991, proposed that the observed acceleration of in-*PWR* fuel cladding corrosion at high burnups (>50 MWd/kgU) might be due to a high hydride density at the metal oxide interface. He even speculated that the rate transition usually observed in out of pile tests might be associated with the onset of hydride precipitation. Hydrides precipitate at a hydrogen concentration in excess of 80-180 wtppm, depending on corrosion temperature.

Kido, 1993 reported on steam corrosion tests at 400°C with Zircaloy-4 samples, precharged in hydrogen/argon gas mixtures to an average content of 100 to 3300 ppm hydrogen, showed a definite acceleration of the corrosion rate for samples with an average hydrogen content exceeding 1000 ppm, Figure 6-1. No information on the distribution of hydrogen/hydrides was given, but increased concentrations at the surface were likely, especially for the samples with a high average H-content. The charging method in these type of experiments is critical to get a hydrogen/hydride distribution in the sample similar to that in irradiated materials.

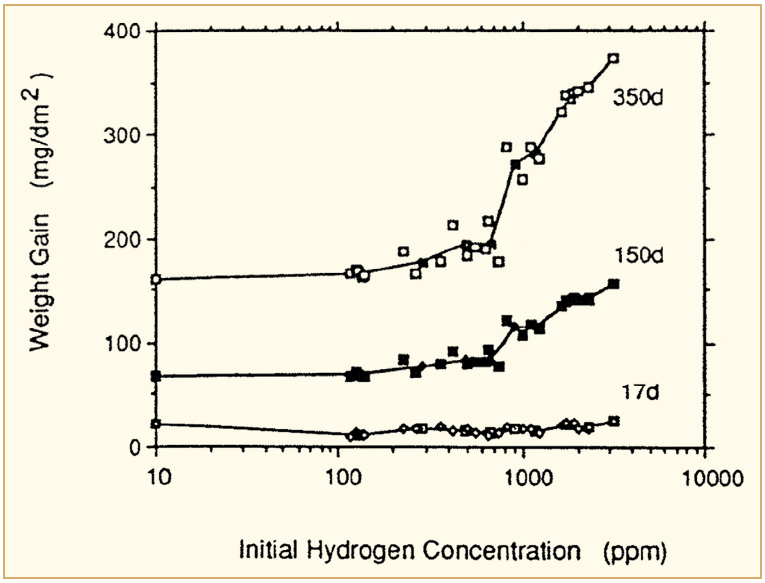

Figure 6-1: Weight gain at 17, 150, and 350 days at 360°C as a function of initial average hydrogen concentration, Kido, 1993.

The detrimental role of hydrogen/hydrides was later confirmed by Blat & Noel, 1995 and Blat et al., 1998. Tests on commercial high Sn (1.5%) cold worked and stress relieved Zircaloy-4 cladding were made that was pre-hydrided by both cathodic and gaseous charging. Their experiments showed a strong increase only for cathodic charged samples (Figure 6-2) with an almost massive hydride rim at the surface and only post-transition (>39 mg/dm², <30 days). A 3 times thicker oxide layer was found for cathodically charged samples at an average H content of 480 ppm, while only a moderate increase, a 50% higher oxide thickness, was found at an average H content of 880 ppm, for gaseous charged samples, after 132 days in 360°C water. The difference in impact on corrosion rate between the different charging methods is because gaseous charging results in hydrides uniformly distributed in the thickness of the sample while cathodic charging results in a massive hydride rim at the *OD* only, Figure 6-3.

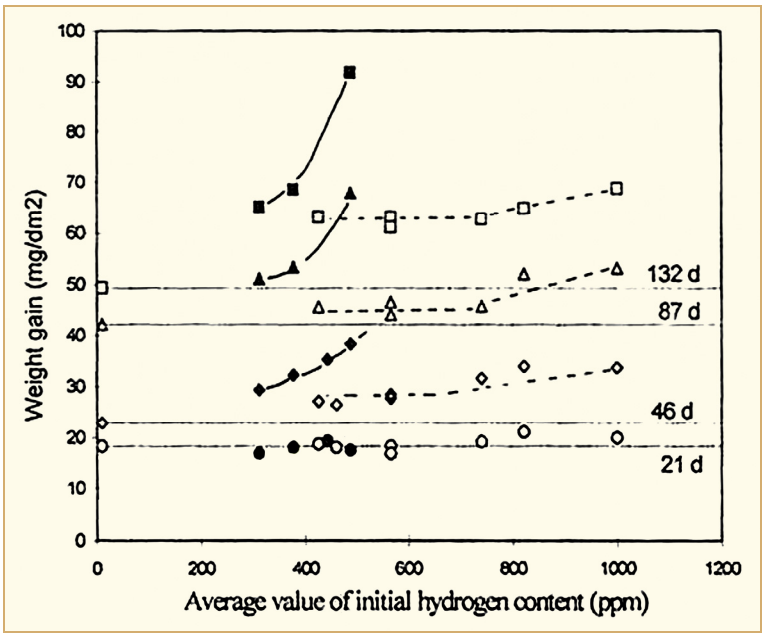

Figure 6-2: Effect of average initial hydrogen content on the corrosion rate in primary light water (2 ppm Li, 1000 ppm B, 360°C), Blat et al., 1998. Filled symbols represent catodhically charged samples and unfilled symbols gaseously charged samples.

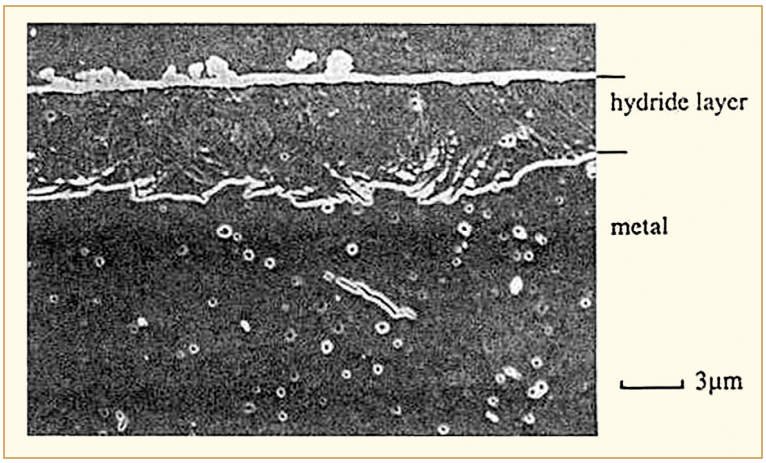

Figure 6-3: *SEM* observation of massive hydride layer just after cathodic charging ([H]: 360 ppm-average concentration), Blat et al., 1998.

Later, it was pointed out, that a significant increase in post-transition corrosion rate only occurs if the hydrogen concentration at the surface is very large (Figure 6-4), ≥8000 ppm, Garzarolli et al., 2001. a hydrogen concentration of 8000 ppm correlates to a 50% dense hydride rim. The samples used for the long term (900 days) corrosion tests in water at 350°C shown in Figure 6-4 had different surface hydrogen contents applied in simulated startup tests in autoclaves, described by Pettersson et al., 2007.

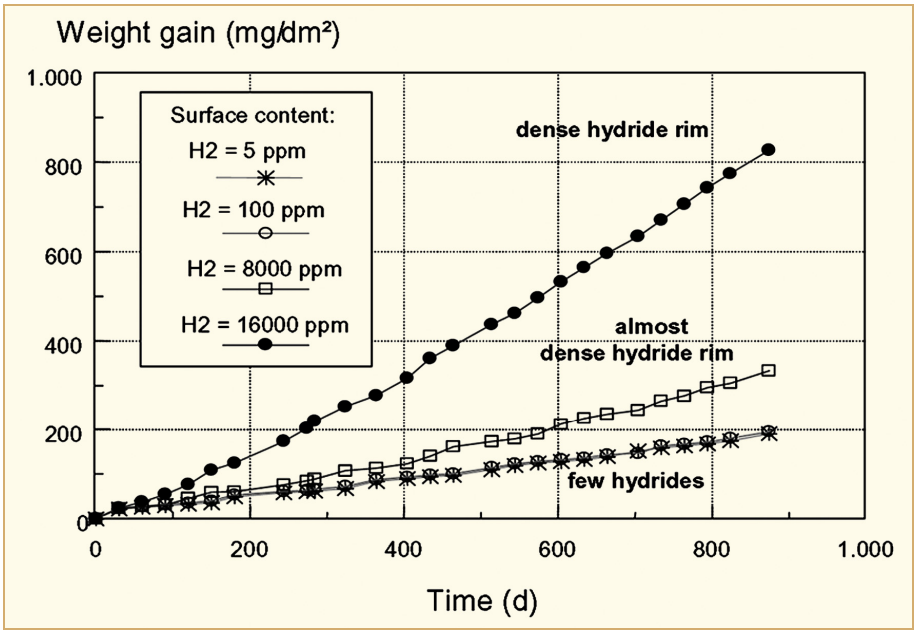

Figure 6-4: Out of pile corrosion of Zircaloy-4 cladding samples with hydride rims in 350°C water, Garzarolli et al., 2001.

Today it is not fully clear if, or under which circumstance, increased corrosion can occur at moderate hydrogen contents (less than several 1000 ppm) at the surface. The information is contradictory. Some tests indicate an increased corrosion rate for concentrations exceeding 800-1000 ppm H, a concentration at which the material surface would be two phase rather than a solid hydride. In any case one can conclude that a solid hydride rim promotes accelerated corrosion due to its lower corrosion resistance and probably by blocking H absorption by the Zr alloy, degrading the protective oxide barrier layer and thereby increasing the corrosion rate further. A two phase α+δ surface, metal with some hydrides, may affect the corrosion rate somewhat, but the data are not clear at this point.

6.3 In-reactor data

As mentioned in Section 4 (Figure 4-19 and Figure 4-20) massive hydride rims can be formed in the fuel cladding at pellet column gaps. At such locations it is generally observed that the corrosion rate is increased although the local temperature at such positions should be significantly lower due to the lower surface heat flux. This in agreement with the finding of Cox & Johnston, 1962 that the water corrosion rate of massive Zr hydrides is larger than that of Zircaloys.

Cheng et al., 1995 concluded from an analytical model that allows separation different parameter effects on corrosion rate such as irradiation, Li, and radial H redistribution – applied to Kido's data that the hydride rim results in a corrosion rate acceleration for a specific 4 cycle *PWR* high burnup fuel rod, Figure 6-5. *This author concluded that it is doubtful that the magnitude of the effect (a factor of 4) is as large as this prediction. Nevertheless modelling is a valuable tool to identify the parameter impact on a specific property and their individual level of importance. Modelling also helps to guide fuel examinations as well as research programs.*

7 Hydride induced dimensional changes

7.1 Mechanisms

All components of fuel assemblies can experience a volume increase as a consequence of corrosion and hydrogen pickup, as was pointed out in Section 2. Theoretically, a hydrogen concentration of 1000 ppm produces about 1% volume increase in Zircaloy, based on the ~16% difference in densities between Zircaloy and zirconium hydride. If this volume increase is assumed to be isotropic, the corresponding linear increase will be 0.33%. Figure 7-1 shows experimental data compared to the "theoretical" relationship. Hydride-induced growth strain appears to be isotopic in the two dimensions measured, but the experimental curve with most hydrides formed at 316°C in unirradiated material, falls significantly below the theoretical curve. This difference could be due to resistance of the metal strained by the hydrides; whereas out-of-pile the relative high yield strength could result in a high resistance, the in-pile resistance, governed by irradiation creep, could be much smaller, depending on the strain rate imposed during hydride precipitation. Also, it could result from a decrease in hydride-induced stress when the material is cooled to room temperature since the coefficient of thermal expansion of hydride is greater than Zr.

It was noted in Section 2 that hydrogen, which occupies interstitial sites in the Zr lattice, causes nearly the same lattice strain as that of the hydride, so there is no change in volume of the zirconium alloy when hydrides may precipitate during cooling to room temperature where hydrogen solubility is close to zero.

The effect of hydrides on dimensional change has been long recognized, e.g., Adamson, 1977, but only recently has the extent been understood. Note that 1000 ppm hydrogen can cause a length change of 12 mm (0.47 inches) in a typical fuel rod or core-length component.

It should also be noted that there is speculation that hydrogen or hydrides may affect the basic irradiation growth processes, Rudling et al., 2007 (page 5-19) perhaps by adding another sink for irradiation-produced defects or by modifying the properties of existing sinks, including <c> component dislocation loops (see Sections 2 and 5.2). Russian data, Figure 7-2, shows a large difference in growth of the E110 alloy depending on whether or not hydrogen absorption occurred ("old E110") or not ("e-E110") during irradiation in the sodium coolant of BOR 60; and data on *PWR* grid (Figure 7-3) or guide tube dimensions, Kesterson et al., 2000 (also discussed below) reveal large dimensional changes. In neither example can hydride-induced volume change explain the differences. Also, for members of the EPRI-sponsored Nuclear Fuel Industry Research (*NFIR*) program, *NFIR* data also implicate hydrides as the cause of unusually high irradiation growth.

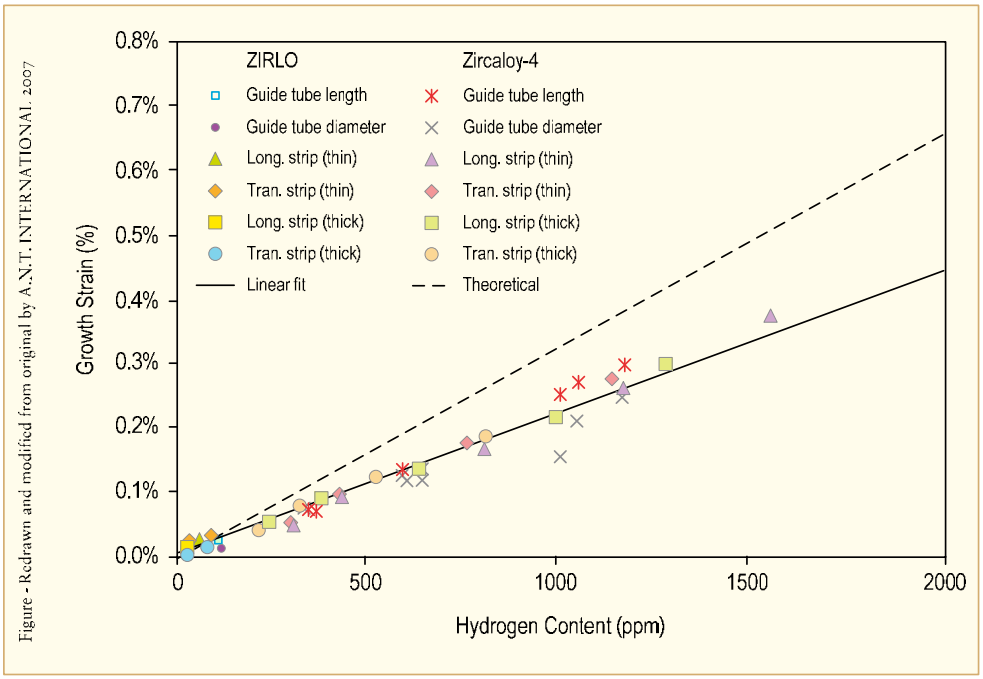

Figure 7-1: Dimensional changes in unirradiated *ZIRLO* and Zircaloy-4 tubing and strip for different sample orientations as a function of hydrogen content, King et al., 2002.

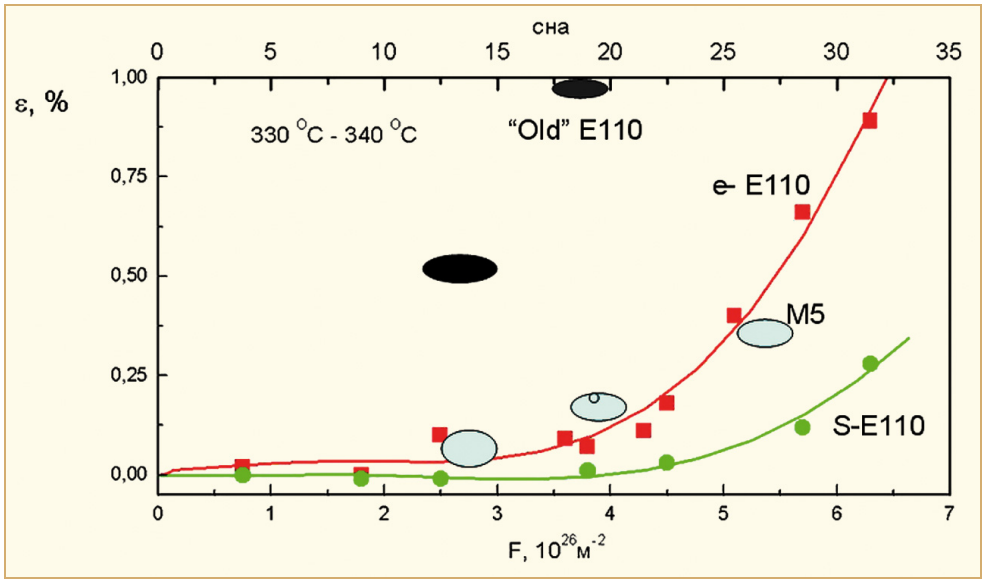

Figure 7-2: Irradiation growth of Zr1Nb alloys as a function of fluence, n/m$_2$ > 01 MeV, at about 330°C (613K). Original data points for electrolytic/Zr iodide e-E110 (red) and sponge S-E-110 (green), Novikov et al., 2006. Data added for M5 (blue), Mardon et al., 2005 and old E110 (black), Shishov et al., 2005. To convert data to n/m$_2$ E>1 MeV in a *PWR* must divide fluence by a factor of 3.3, Shishov et al., 2005.

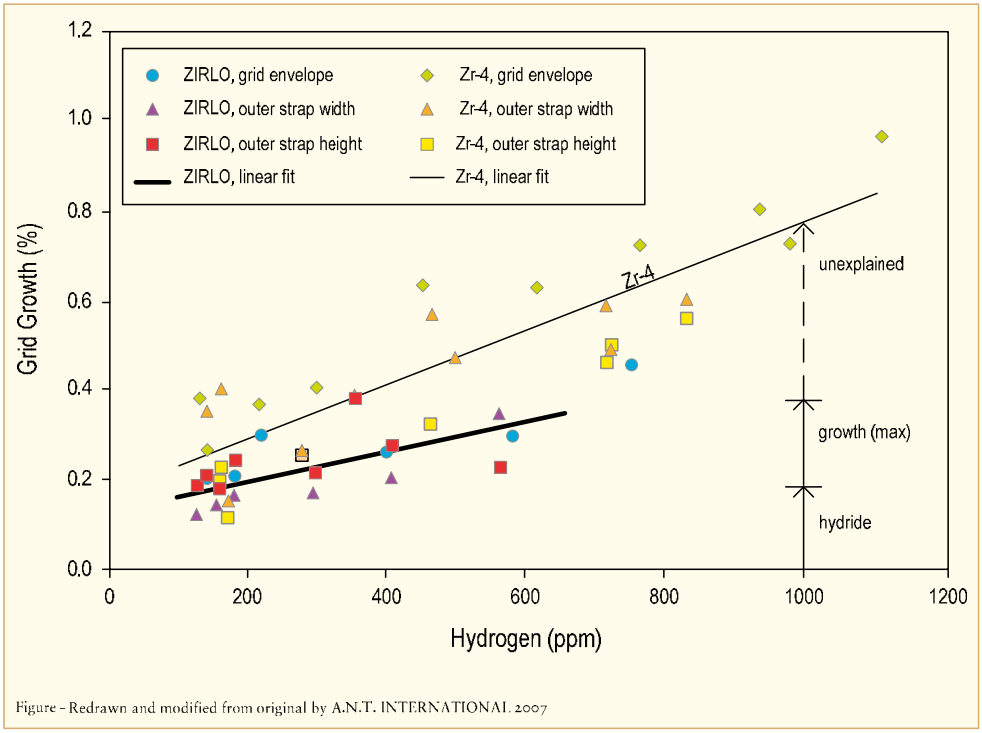

Figure 7-3: Grid dimensional changes as a function of measured hydrogen content. Neutron fluence is constant over the hydrided regions. King et al., 2002. The 3 components of grid growth (hydride, maximum growth and unexplained) have been estimated by R. Adamson.

7.1.1 *BWR* cladding results

BWR fuel rods with *LK2* claddings, with very fine *SPP*, have shown increased hydrogen pickup, oxide layer build up, and length growth at burnups in excess of 30 MWd/kgU, Figure 7-4. From the growth behaviour of different fuel rods which were examined for their hydrogen content the hydrogen induced rod growth of *LK2* claddings was deduced versus the measured hydrogen content, after correction for the expected irradiation induced growth, Figure 7-5. The hydrogen induced growth indicated by the figure is about 50% larger than the values estimated from the theoretical density increase (0.33% per 1000 ppm H). Thus it can be speculated, that parameters other than the density difference contribute to the observed rod growth, including possible pellet-cladding-mechanical-interaction.

8 Effect of hydrogen on mechanical properties

8.1 Introduction

The relationship of the mechanical test conditions that measure the effect of hydrides to the actual fuel performance conditions to be evaluated need to be established if the mechanical test conditions and results are to provide meaningful data. While this task is beyond the scope of this report, a brief guide to put the mechanical test results in this section into the context of performance conditions seems appropriate.

The exact simulation of fuel performance conditions by testing is difficult if not impossible, whether they be normal in-reactor operation, hypothetical accident conditions or spent fuel storage. This gives rise to the task of interpreting the test conditions and test results for their valid application to either evaluating or predicting the performance under these conditions. Consideration must be given to the variety of factors influencing these conditions that involve different stress levels, stress distributions, strain rates, temperatures, component shapes, material characteristics and irradiation effects.

An approach to this is the review of the vendors' mechanical design for the component in question including his design basis. These data will obviously vary from design to design and from vendor to vendor. Some generic examples are given below as examples for the various factors to be considered.

Stresses and stress distribution

The *tensile strength and yield strength* of materials is routinely measured by uniaxially stressed tensile specimens. The data apply primarily to the structural members of the assembly and in a limited way to the cladding. The majority of the critical stresses in the cladding tubing are the result of either their internal pressurization or the pressure differential across their wall. Tubular specimens under biaxial stresses that simulate internal pressure or localised stress are the appropriate way to evaluate these.

Burst strength is evaluated by internal pressurization of tubular specimens.

If possible, the simulation of *stress distribution* in a component is important, especially if concentrations of hydrides in the sample are involved. Verification by finite element analyses provides valuable insight.

The *strain rates* applied are critical to obtain representative results. The extremes are slow strain rates for *creep* simulating dry storage or cladding creepdown in-reactor and very rapid rates for simulating *RIA*. Stresses assumed due to lateral impacts during seismic event analyses can be sufficiently complex to require special rigs for testing and involve *impact strength* evaluation, also a high strain rate test.

The effects of *cyclic stresses* have been evaluated as they might apply to vibration of spacers and channels due to hydraulic effects and cladding due to power cycling. The large margins to limits and low event probability have made this a less significant case. For more details see *IZNA1/ZIRAT6* Report on Mechanical Properties, Adamson & Rudling, 2001.

The application of *fracture toughness*, resistance to crack propagation, can apply to cladding during *RIA* events or perhaps to other components with incipient cracks. This particular property has not been a part of fuel design bases in the past, but may be valuable in the evaluation of performance results. The development of specimens representative of plane strain in tubular cladding has been a key need to obtain representative results. *Impact testing* has also been used for this purpose.

Ductility

The impact of hydrides on Zr alloy ductility is perhaps the most important property to be evaluated, since the resulting decrease in ductility is a major issue. Ductility is also one of the most difficult properties to define, particularly for a two phase material, such as Zr metal matrix + Zr hydrides, with a non-uniform ductility. The material can have good ductility in the matrix between hydride particles and poor ductility in the hydrides, all on a microscopic scale. (This ignores any potential effect of *SPP*s.) The gauge length used in the test becomes important since it defines the material being tested. The usual, relatively long gauge lengths of 10-50 mm can involve a mixture of phases or phase concentrations and the test can produce results that represent the average ductility of the phases, or the ductility of one or the other, depending on the phase and stress distributions. And, irradiation induces marked in-homogeneous deformation on a microscopic scale. The results therefore can be questionable. Small gauge lengths and micro-specimens that represent conditions at the potential crack tip are clearly more desirable. For more details, see *IZNA1/ZIRAT6*, Adamson & Rudling, 2001.

Evaluation of the ductility on a micro-scale can give valid results, but these may not answer the needs of an engineering evaluation of the material. Hence each application of a ductility requirement should be tailored to the specific component and its performance requirements. The ductility values can be interpreted as *uniform elongation, total elongation, or reduction-in-area* depending on the application and whether the material is irradiated or un-irradiated.

Temperature

The applicable temperatures will depend primarily on the service environment and to some degree on the fuel design. For *normal operation* the cladding temperatures will vary from the hot inside to the cool outside in the range of about 280-400°C for *PWR*s and 270-350°C for *BWR*s. Structural materials will be slightly above the coolant temperatures due to gamma heating, the coolant temperatures being about 280-330°C for *PWR*s and 270-300° for *BWR*s from inlet to outlet in each case. Temperature histories will depend on the operating mode.

The time-temperature history of the test can have an effect on the hydrogen distribution in the sample, as well as on the annealing of the irradiation effects, as noted below.

For *hypothetical accidents* the temperatures and temperature histories will be dependant on the accident scenario assumed and the reactor system and fuel designs as well, but generally will be quite short in duration.

The *dry cask storage* temperature history will affect the cladding primarily, and will start in the 300-400°C range and decrease over several decades with the concurrent decrease in stresses. The structural materials will be at a much lower temperature.

The *handling and transport* of fuel will occur at low or room temperature and that is an important consideration since the ductility of the hydrided Zr alloys will then be at its lowest.

Materials

The materials to be tested should be as close if not identical, to the materials being evaluated and applied for the fuel assemblies intended for use. This is not a problem when taking test samples from fuel assemblies that have been irradiated. If that is not the case, however, then care must be taken to select materials that have the same composition, the same fabrication history and the same shape as the component of interest. As an example, sheet samples have been used to evaluate the effect of H on mechanical properties in numerous instances, sometimes matching the texture of tubing and sometimes not. Care must be taken in applying such data to cladding.

A large fraction of the data on the effect of H on mechanical properties has been tested on unirradiated, pre-hydrided samples. The hydriding procedure itself can have difficulties in reproducing H distributions typical of in-reactor service, so this should be evaluated as well.

Effects of irradiation

The effects of irradiation hardening on the Zr alloys should be included in most mechanical property evaluations. In-reactor mechanical testing, expensive and rarely done, will account for this parameter. Ex-reactor testing may or may not anneal out the effects due to radiation damage. For more details see, Adamson, 2006. Tests at room temperature and relatively low temperatures will maintain the effects of irradiation. Tests at elevated temperatures, greater than about 350°C can anneal out the radiation effects depending on the time-temperature history of the test and the metallurgical condition of the material (recrystallized or cold worked). As an example, this would be applicable to long term ex-reactor dry storage conditions to simulate in-reactor creep tests of irradiated materials. This sentence does not seem to correlate with the next sentence. The creep data would not be applicable to evaluate in-reactor cladding creep-out due to internal pressure; annealing out the radiation damage would increase the creep rate in the ex-reactor test compared to the creep rate that would be present in-reactor.

These brief examples are meant to re-emphasize the importance of evaluating the applicability of the mechanical test conditions and results to the design and performance of the fuel assembly components.

8.2 Mechanical properties of hydrides

8.2.1 Introduction

The amount of hydrides in the Zr alloys can vary from a low level, uniform dispersion to regions of solid hydrides and as a result will have varying effects on the mechanical properties of the alloys. The properties of the hydrides themselves are important therefore, since they can affect the performance of hydrided Zr alloys. Their mechanical properties are summarized in this section. The physical properties of the hydrides were summarized in Section 2.3.

8.2.2 Density

The density of the Zr hydrides is lower than that of Zr metal and decreases as a function of increasing H content, Figure 8-1. The most commonly observed δ hydride, $ZrH_{1.66}$, has a density of about 5.65 compared to 6.5 g/cc for Zr metal, about 13% lower. This will result in a volume expansion, whether H is in solid solution or as a hydride, resulting in internal stresses and dislocations surrounding the hydride. The volume expansion due to hydrides has been estimated in the range of 14 – 17%, Coleman, 2003, and results in the dimensional growth, discussed in Section 7.

Mechanical property data on solid hydrides are scarce. The specimens are difficult to prepare because of their brittle nature and their decreased stability in high temperature tests. Nevertheless, these are important data in order to answer the questions on the ductility of hydrides at elevated temperatures and the definition of the temperature at which they no longer affect the ductility of Zr alloys.

9 References

Adamson R. B., "*Irradiation Growth of Zircaloy*", Zirconium in the Nuclear Industry; Third Conference, *ASTM* STP 633, pp. 326, *ASTM*, 1977.

Adamson R.B. and Rudling P., "*Mechanical Properties of Zirconium Alloys*", *IZNA1/ZIRAT6* Special Topics Report, 1991.

Adamson R. B., Lutz D. R., Davies J. H., "*Hot Cell Observations of Shadow Corrosion Phenomena*", Proceedings Fachtagung der KTG-Fachgruppe, Brennelemente und Kernbautelle", 29 Februar/1 Marz 2000, Forschungszentrum Karlsruhe, 2000.

Adamson R. B. and Rudling P., "*Mechanical Properties of Zirconium Alloys*", *IZNA1/ZIRAT6* Special Topical Report, ANT International, November, 2001.

Adamson R. B., "*Recovery of Irradiation Damage by Posts-Irradiation Thermal Annealing-Relevance to Hydrogen Solubility and Dry Storage Issues*", EPRI Technical Report 1013446, June 2006.

Adamson R., Cox B., Garzarolli F., Sabol G. Strasser A. and Rudling P., *IZNA7/ZIRAT12* Annual Report, 2007.

Aitcheson I., "*Effect of orientation of hydride precipitates on the fracture toughness of cold worked Zircaloy-2 and Zr2.5 Zirconium*", Applications-related Phenomena for Zirconium and its Alloys, *ASTM* STP 458, *ASTM*, pp 160-178, 1969.

Alam A. M and Hellwig C., "*Cladding Tube Deformation Test for Stress Reorientation of Hydrides*", Zr in the Nuclear Industry, 15th International Symposium, Sunriver (OR), June 25th-28th, 2007.

Andersson B.,"*BWR Fuel Experience*", *ANT* International -Westinghouse Information Meeting, December 2, 2005.

Aomi M. et al., "*Evaluation of Hydride Reorientation Behavior and Mechanical Property for High Burnup Fuel Cladding Tube in Interim Dry Storage*", Zr in the Nuclear Industry, 15th International Symposium, Sunriver (OR), June 25th-28th, 2007.

Arborelius J., Dahlbäck M., Hallstadius, L., Jourdain P., et al., "*The Effect of Duplex Cladding Outer Component Tin Content on Corrosion Hydrogen Pick-up and Hydride Distribution at Very High Burnup*", 14th Int. Symposium on Zirconium in the Nuclear Industry, Stockholm, Sweden, p. 526, STP 1467, 2004.

Arsene S. and Bai J., "*Effect of hydriding and irradiation on the mechanical properties of Zircaloy cladding*", CRNS URA Report No. 850, 1998.

Arséne S., Bai J. and Bompard P., "*Hydride Embrittlement and Irradiation Effects on the Hoop Mechanical Properties of PWR and BWR Zircaloy Cladding Tubes, Part 1*", Metallurgical and Materials Transactions, v. 34A, p. 532-556, March 2003.

Asher R. C. and Trowse F. W., "*The Distribution of Hydrogen in Zirconium Alloy Fuel Cladding: The Effects of Heat Flux*", J. Nucl. Mat. 35, p.115-121, 1970.

Bai J. B., "*Influence of an oxide layer on the hydride embrittlement in Zircaloy-4*", Scripta Metallurgica at Material, 29, pp 617-622, 1993.

Bai J. Gilbon J., Prioul C. and Francois D., "*Hydride Embrittlement in Zircaloy-4 Plate, Part I Influence of Microstructure on the Hydride Embrittlement in Zircaloy-4 at 20°C and 350°C" and "Part II, Interaction Between the Tensile Stress and the Hydride Morphology*", Met. and Materials Transactions, v. 25A, June, 1994.

Bai J., "*Effect of Hydriding Temperature and Strain Rate on the Ductile-Brittle Transition in β Treated Zircaloy-4*", Journal of Nuclear Science and Technology, v. 33, No.2, p. 141-146, February, 1996.

Barberis P., Rebeyrolle V., Vermoyal J.J., Chabretou V. and Vassault, J.P., "*CASTA DIVTM: experiments and modeling of oxide induced deformation in nuclear components*", 15th *ASTM* International Symposium: Zirconium in the Nuclear Industry, Sun River, OR, June 2007.

Barraclough K. G., and Beevers C. J., "*Some observations on deformation characteristics of bulk polycrystalline zirconium hydride: Part 1 The deformation and fracture of hydrides based on the delta phase*", J. Materials Science, 4, pp. 518-525, 1969.

Beck R. and Mueller W., "*Mechanical Properties of Solid Zirconium Hydride*", Nuclear Metallurgy: A Symposium on Metallic Moderators and Cladding Materials, Vol. VII, p. 65, AIMMPE, New York, Oct. 1960.

Beck R., "*Thermophysical Properties of Zirconium Hydride*", American Society of Metals, Trans. Quart. v.55, p. 556, 1962.

Berry E. B. et al., "*Hydrogen pickup during aqueous corrosion of Zr alloys*", Corrosion Vol. 17, pp. 109t-117t, 1961.

Bertolino G., Meyer G. and Ipiña J. Perez, (a) "*Effects of Hydrogen Content and Temperature on Fracture Toughness of Zircaloy-4*", Journal of Nuclear Materials, v. 320, p.272, 2003. (b) "In-Situ Crack Growth Observation and Fracture Toughness Measurement of Hydrogen Charged Zircaloy-4", Journal of Nuclear Materials, v. 322, p. 57, 2003.

Bertolino G., Perez Ipina J. and Meyer G., "*Influence of the Crack-Tip Hydride Concentration on the Fracture Toughness of Zircaloy-4*", Journal of Nuclear Materials, 348, 205-212, 2006.

Besch O., Yagnick S., Woods K., Eucken C., et al., "*Corrosion Behavior of Duplex and Reference Cladding in NPP Grohnde*", 11th Int. Symposium on Zirconium in the Nuclear Industry, Garmisch-Partenkirchen, Germany, p. 805, *ASTM* STP 1295, 1995.

Bickel P., "*Measurement and Interpretation of Electrical Properties, of Zirconium Hydride*", NAA-SR-1173, Jan. 1960.

Bickel P., Berlincourt, Physical Review, B2, 4807, 1970.

Blat M. and Noel D., "*Detrimental Role of Hydrogen on the Corrosion Rate of Zirconium Alloys*", 11th Int. Symposium on Zirconium in the Nuclear Industry, Garmisch-Partenkirchen, Germany, p. 319, *ASTM* STP 1295, 1995.

Blat M., Legras, L., Noel, D., Amanrich, H., "*Contribution to a Better Understanding of the Detrimental Role of Hydrogen on the corrosion Rate of Zircaloy-4 Cladding Materials*", 12th Int. Symposium on Zirconium in the Nuclear Industry, Toronto, Canada, p. 563, *ASTM* STP 1354, 1998.

Blavius D, Munch C-J and Garner N.L., "*Dimensional Behavior of Fuel Channels – Update on the operational Experience and Evaluation Results*", KTG, 2007.

Blavius D et al., "*Dimensional Behavior of Fuel Channels – Update on the operational Experience and Evaluation Results*", Proc. Annual Meeting on Nuclear Technology, Deutsches Atomforum, pp. 451-459, Hamburg, Germany, 2008.

Bossis P., Thomazet J. and Lefebvre F., "*Study of the Mechanisms Controlling the Oxide Growth Under Irradiation: Characterization of Irradiated Zircaloy-4 and Zr-1Nb-O Oxide Scales*", Zirconium in the Nuclear Industry: Thirteenth International Symposium: *ASTM* STP 1423, G. D. Moan and P. Rudling, Eds., *ASTM* International, pp. 190-221, West Conshohocken, PA, 2002.

Bossis P. et al., "*Comparison of the high burnup corrosion of M5 and Low-Tin-Zry-4*"; *ASTM* STP 1467, pp. 494-524, 2006.

Bossis P., Verhaeghe B., Doriot S., Gilbon D., Chabretou V., Dalmais A., Mardon J.P., Blat M. and Miquet A., "*In PWR Comprehensive Study of High Burn-up Corrosion and Growth Behavior of M5 and Recrystallized Low-Tin Zircaloy-4*", 15th *ASTM* International Symposium: Zirconium in the Nuclear Industry – Sun River, OR, June 25-27, 2007.

Bouffioux P. and Rupa N., "*Impact of Hydrogen on Plasticity and Creep of Unirradiated Zircaloy-4 Cladding Tubes*", 12th Int. Symposium on Zirconium in the Nuclear Industry, Toronto, Canada, p. 399-422, *ASTM* STP 1354, 1998.

Bouffioux P. and Legras L., "*Effect of hydriding on the residual cold work recovery and creep of Zircaloy 4 cladding tubes*", Proc: ANS conference on fuel performance, Park City, USA, 2000.

Brown A. and Hardie D., "*The Effect of Dissolved Oxygen on the Terminal Solubility of Hydrogen in Alpha Zirconium*", Journal of Nuclear Materials, v. 4, No. 1, p. 110-112, 1961.

Broy Y., Garzarolli F., Seibold A. and Van Swam L. F., "*Influence of Transition Elements Fe, Cr, and V on Long-Time Corrosion in PWRs*", Zirconium in the Nuclear Industry: 12th Int'l Symposium, *ASTM* STP 1354, G. P. Sabol and G. D. Moan, Eds., *ASTM*, West Conshohocken, PA, 609-622, 2000.

Cann C., Puls M., Sexton E. and Hutchings W., "*The Effect of Metallurgical Factors on Hydride Phases in Zirconium*", Journal of Nuclear Materials, v. 126, p. 197, 1984.

Cappelaere C., "*Long Term Behavior of Spent Fuel Cladding in Dry Storage Conditions*", ICEM 2001, Bruges, Belgium, October, 2001.

Carpenter G., Watters, J. and Gilbert R., "*Dislocations Generated by Zirconium Hydrides in Zirconium and some of its Alloys*", Journal of Nuclear Materials, v. 48, p267, 1973.

Chabretou V. and Mardon J.P., "*M5 alloy high burnup behaviour*", KTG Fachtag on Status of *LWR* Fuel Development and Design Methods, Dresden, March 2-3, 2006.
Charquet D. et al., "*Hydrogen absorption kinetics during Zircaloy oxidation in steam*", *ASTM* STP 1245, pp. 80-97, 1994.
Cheng B., Gilmore P. and Klepfer H., "*PWR Zircaloy Fuel Corrosion Performance, Mechanisms and Modeling*", 11th Int. Symposium on Zirconium in the Nuclear Industry, Garmisch-Partenkirchen, Germany, p. 137, *ASTM* STP 1295, 1995.
Cheng B., Smith D., Armstrong E., Turnage K. and Bond G., "*Water Chemistry and Fuel Performance in LWRs*", Int. Conference on *LWR* Fuel Performance, Park City, Utah, p. 355, ANS, 2000.
Chirigos J.N. et al., "*Fuel element fabrication with special emphasis on cladding materials*", Symposium on Fuel Elements, Vienna, May 1960.
Christensen H. et al., "*Experimental studies of radiolysis in an in-core loop in the Studsvik R2 reactor*" Proc. BNES conference on Water Chemistry of Nuclear Reactors Systems, pp. 483-485, 1996.
Chu H. C., Wu S. K., Kuo R. C. and Cheng S. C., "*Effect of Radial Hydrides on Mechanical Properties of Zircaloy-4 Cladding*", Proc. Water Reactor Fuel Performance Meeting, Kyoto, Japan, October 2-6, 2005.
Chu H. C, Wu S. K, Kuo R. C, "*Hydride reorientation in Zircaloy-4 cladding*", Journal of Nuclear Materials, vol.373, p. 319, 2008.
Chung H., Daum R., Miller J. and Billone M., "*Characteristics of Hydride Precipitation and Reorientation in Spent-Fuel Cladding*", 13th International Symposium in Zirconium in the Nuclear Industry, Annecy, France, p. 561, *ASTM* STP 1423, 2002.
Coleman C. and Hardie D., "*The Hydrogen Embrittlement of Zirconium in Slow Bend Tests*", Journal of Nuclear Materials, v. 19, p. 1, 1966.
Coleman C., "*Effect of texture on hydride reorientation and delayed hydrogen cracking in cold worked Zr-2.5Nb*", *ASTM* STP 754, pp. 393-411, 1982.
Coleman C. E. and Ambler J. F. R, "*Solubility of Hydrogen Isotopes in Stressed Hydride – Forming Metals*", Scripter Met. 17, pp. 77-82, 1983.
Coleman C. E., "*Cracking of hydride-forming metals and alloys*", Comprehensive Structural Integrity, Vol. 6, Environmentally Assisted Failure, F. Petit and P. Scott, Eds, chapter 6-03, pp. 103-161, 2003.
Cox B. and Johnston T., v. 18, p.33, Corrosion, 1962.
Cox B., "*Oxidation of Zirconium and Its Alloys*", Advances in Corrosion Science and Technology, Vol. 5, Edited by Mars G. Fontana and Roger W. Staehle, Plenum, N. Y., pp. 173--391, 1976.
Cox B. and Ling V. C., "*Effect of thermal-cycling on the movement of the (α-Zr+$ZrH_{1.6}$) phase boundary in Zr2.5Nb*", *AECL*-6538, pp. 73-78, 1979.
Cox B., "*Assessment of in-reactor corrosion models and data for Zircaloys in water*", Proc. 2nd Int. Symp. on Environmental Degradation of Materials in Nuclear Power Systems-Water Reactors, pp. 219-226, Montery, Ca., USA, 1985.
Cox B., "*Hydrogen trapping by oxygen and dislocations in zirconium alloys*", J. Alloys and Comp., Vol. 256, pp.L4-L7, 1997.
Cox B. and Wong Y.M. "*A hydrogen uptake micro-mechanism for Zr alloys*", J. Nucl. Mat. Vol. 270, pp. 134-146, 1999.
Cox B. and Rudling P., "*Hydriding Mechanisms and Impact on Fuel Performance*", Advanced Nuclear Technology for *ZIRAT5*, 2000.
Cupp C. R. and Flubacher P., J. Nuclear Mater., Vol. 2, pp. 213-228, 1962.
Daum R., Bates D., Koss A. and Motta A., "*The Influence of a Hydrided Layer on the Fracture of Zircaloy-4 Cladding Tubes*", Int. Symposium on Hydrogen Effects on Materials Behavior and Corrosion Deformation Interaction, Moran Wyoming, TMS, September, 2002.
Daum Robert S., Majumdar Saurin, Liu Yung and Billone Michael C., "*Mechanical Testing of High-Burnup Zircaloy-4 Fuel Cladding under Conditions Relevant to Drying Operations and Dry-Cask Storage*", Proc. Water Reactor Fuel Performance Meeting, pp. 498-531, Kyoto, Japan, October 2-6, 2005.